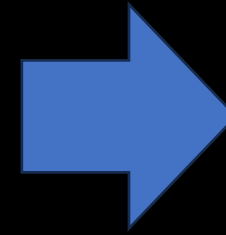
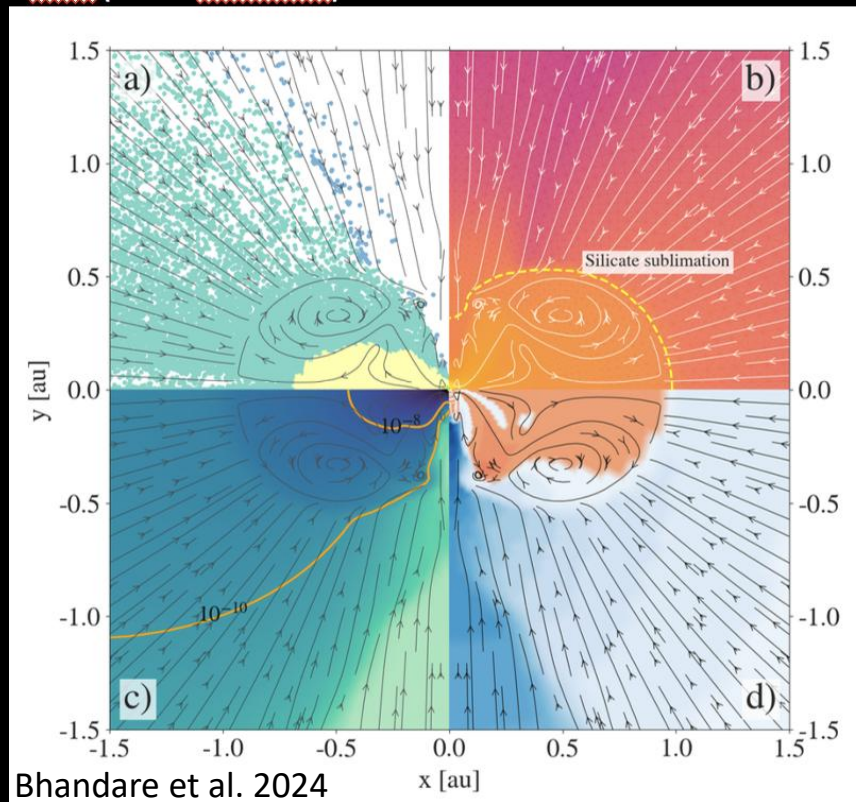


Out of equilibrium condensation processes In the Solar Nebula: from thermodynamics to MHD simulations



Primitive meteorites (chondrites) are divided in 3 « broad » classes

Enstatite C.



Ordinary C.



Carbonaceous C.



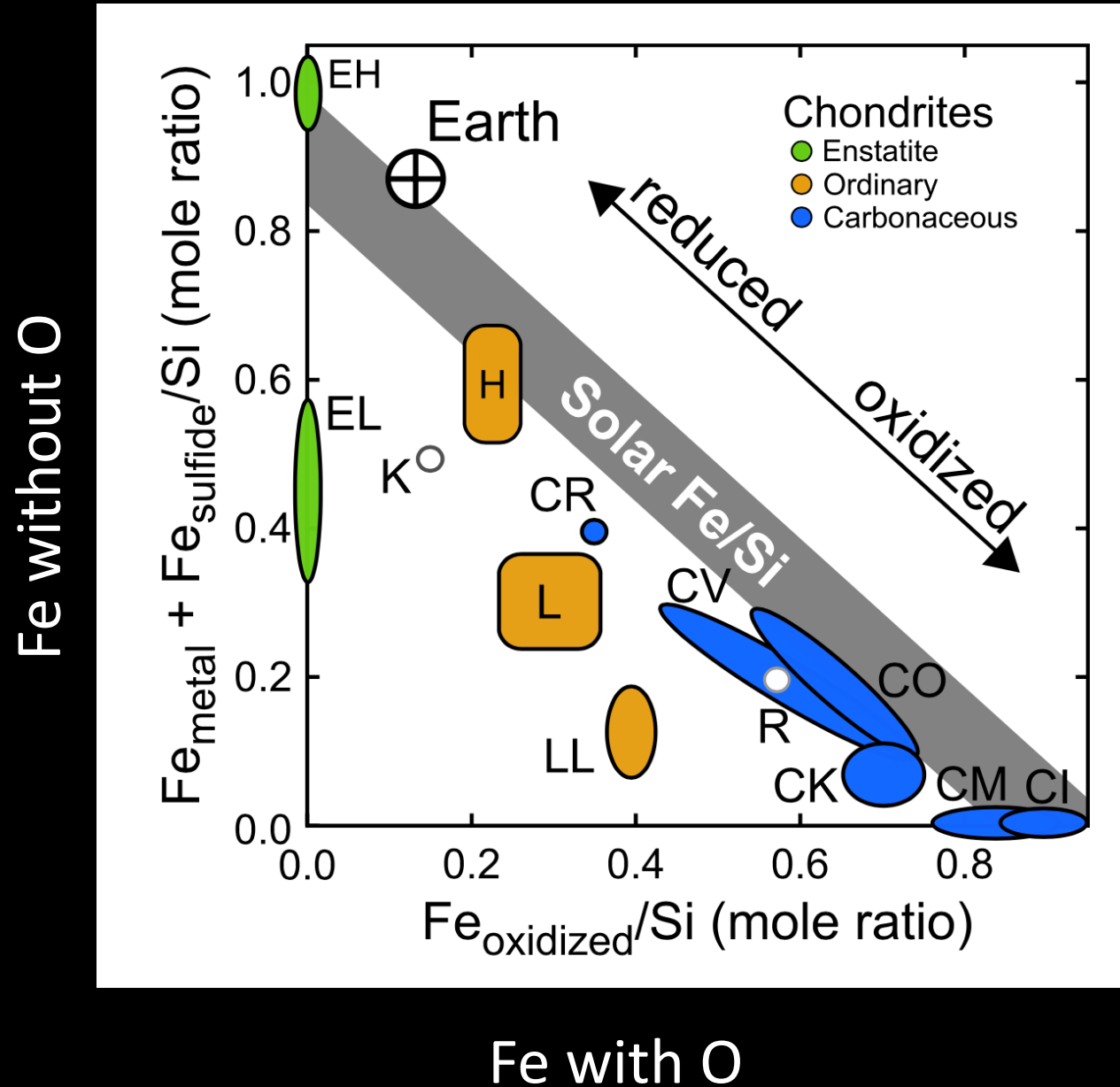
Iron oxidation level

Enstatite

Olivine (Forst., Faya)

Refractory atoms + CAIs

The Urey-Craig Diagram (1953) : a proxy for the oxidation state of chondrites

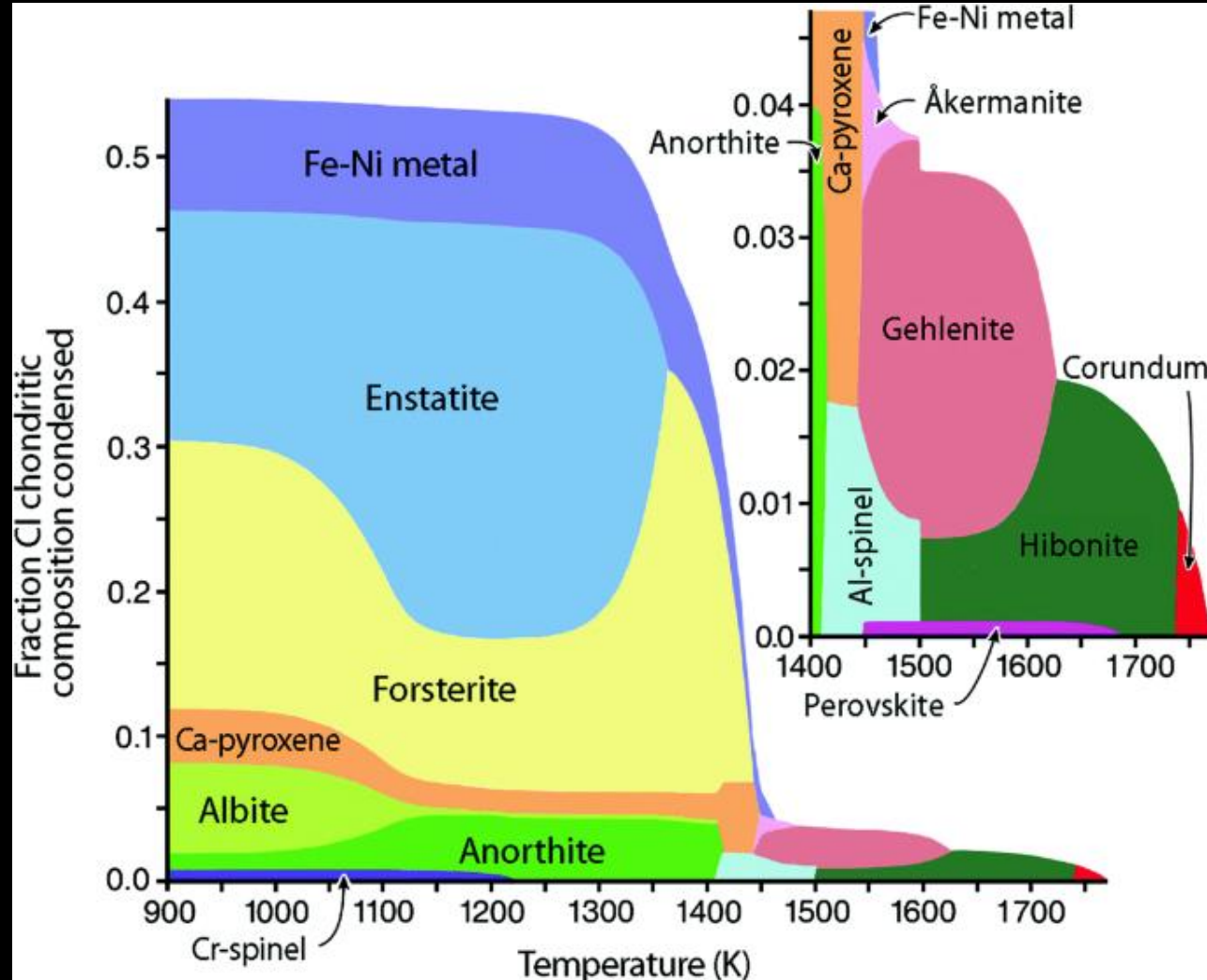


(Urey & Craig, 1953)
adapted from
Yoshizaki et al. (2021)

- Discontinuous mineralogies

The « Equilibrium Condensation Sequence »

Grossman 1972, and many others... Woitke et al., 2016, Ebel et al., 2023



Gas of Solar composition

Minimization of Gibbs free energy =>

Chemical equilibrium=>
« most stable minerals »

=> **NON –EQUILIBRIUM MUST BE INTRODUCED =>**

=> Fractionated condensation , isolation factor

=> (Work of Petaev)

=> Importance of secondary processes.

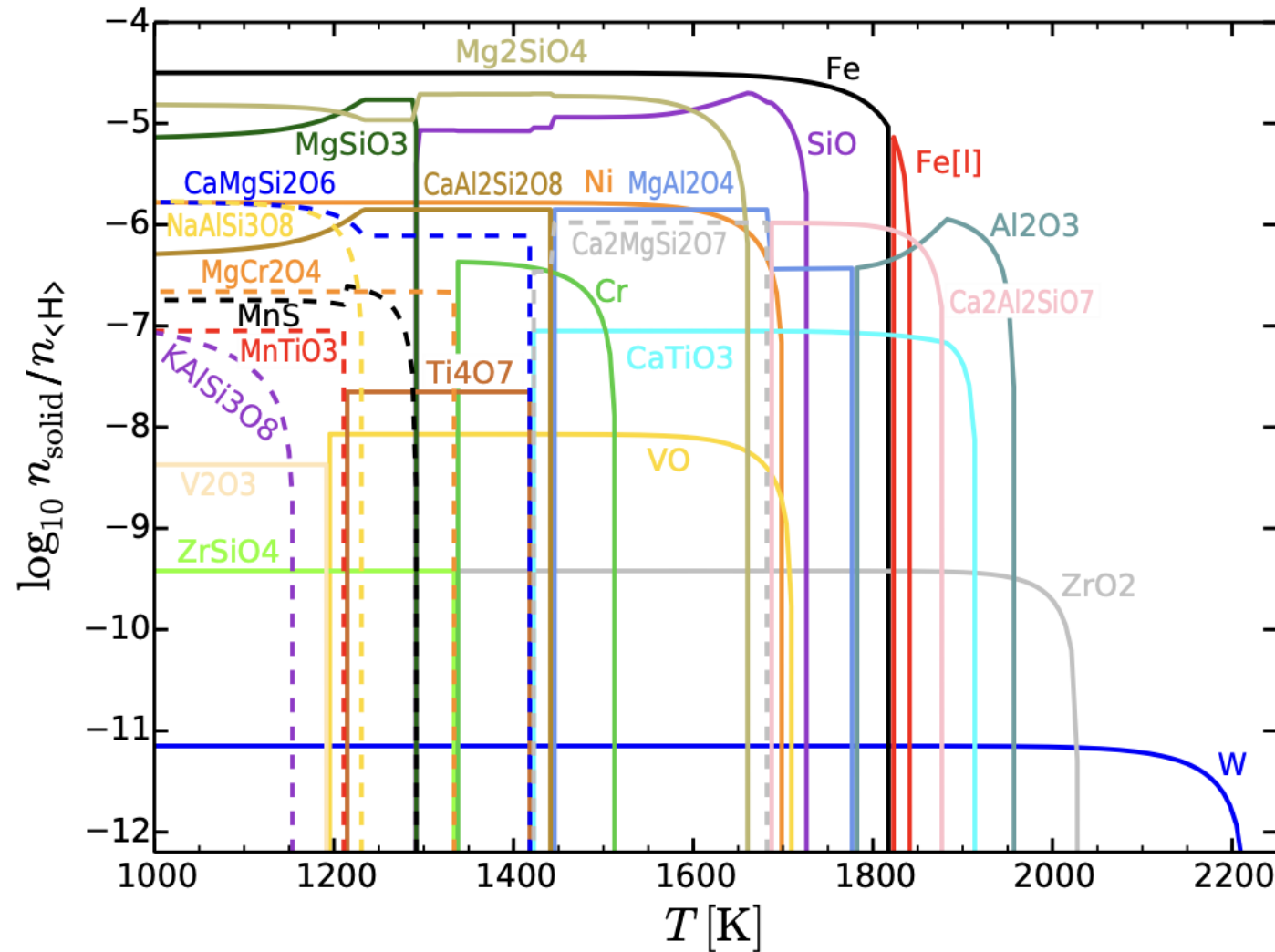
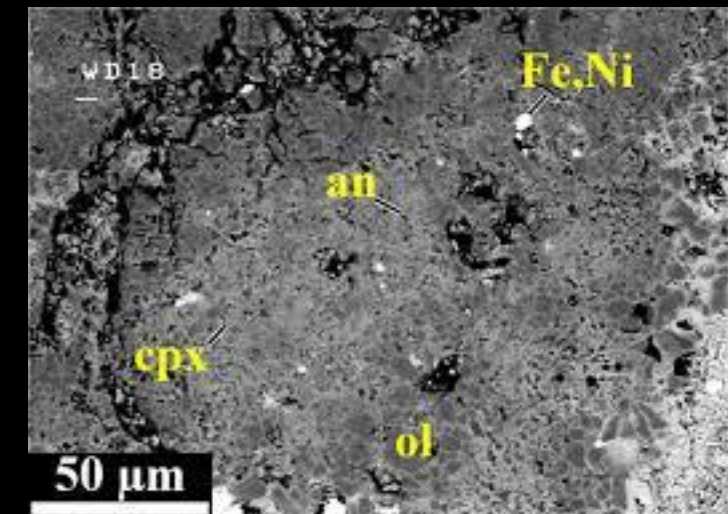
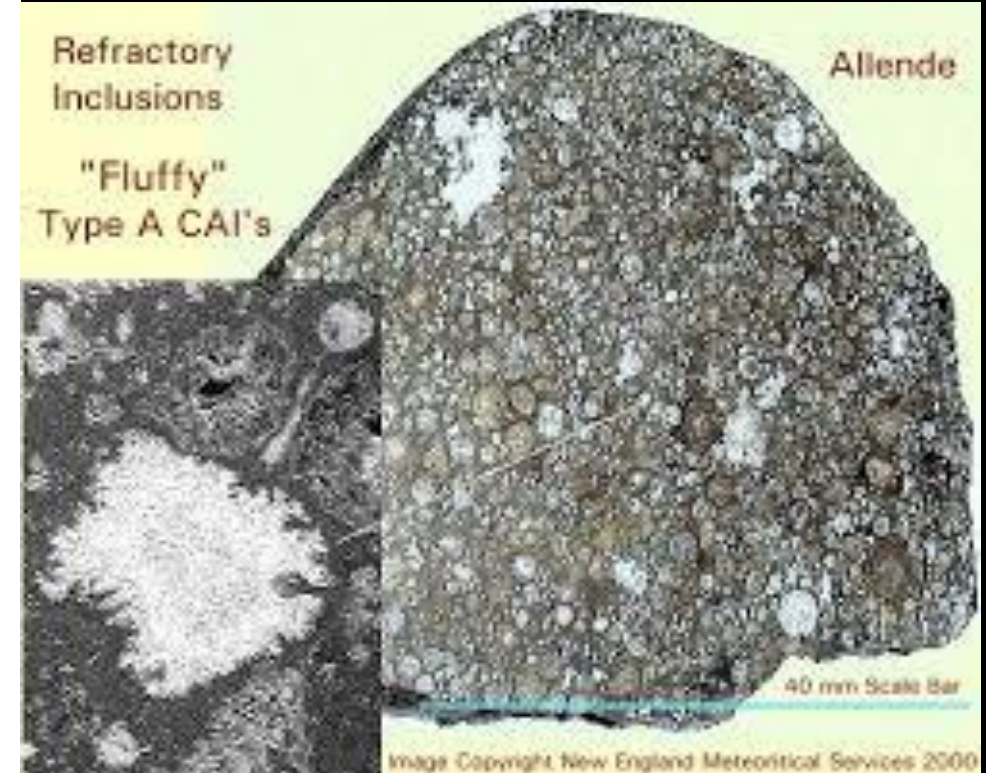


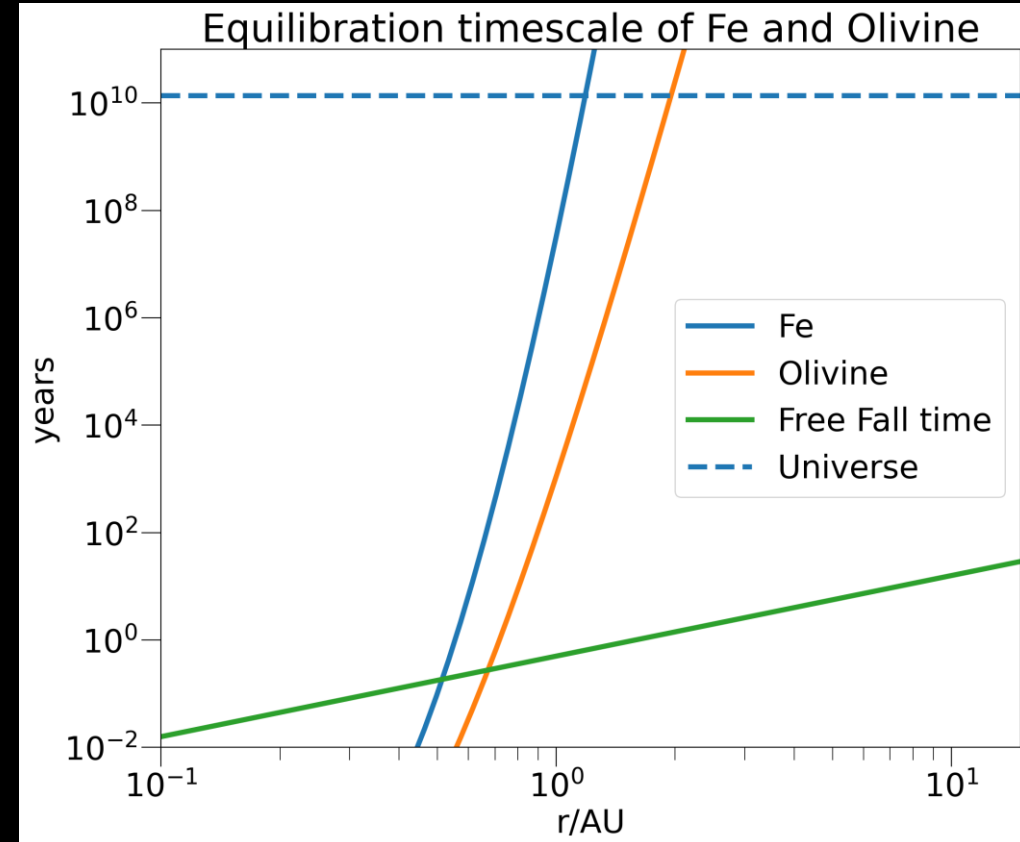
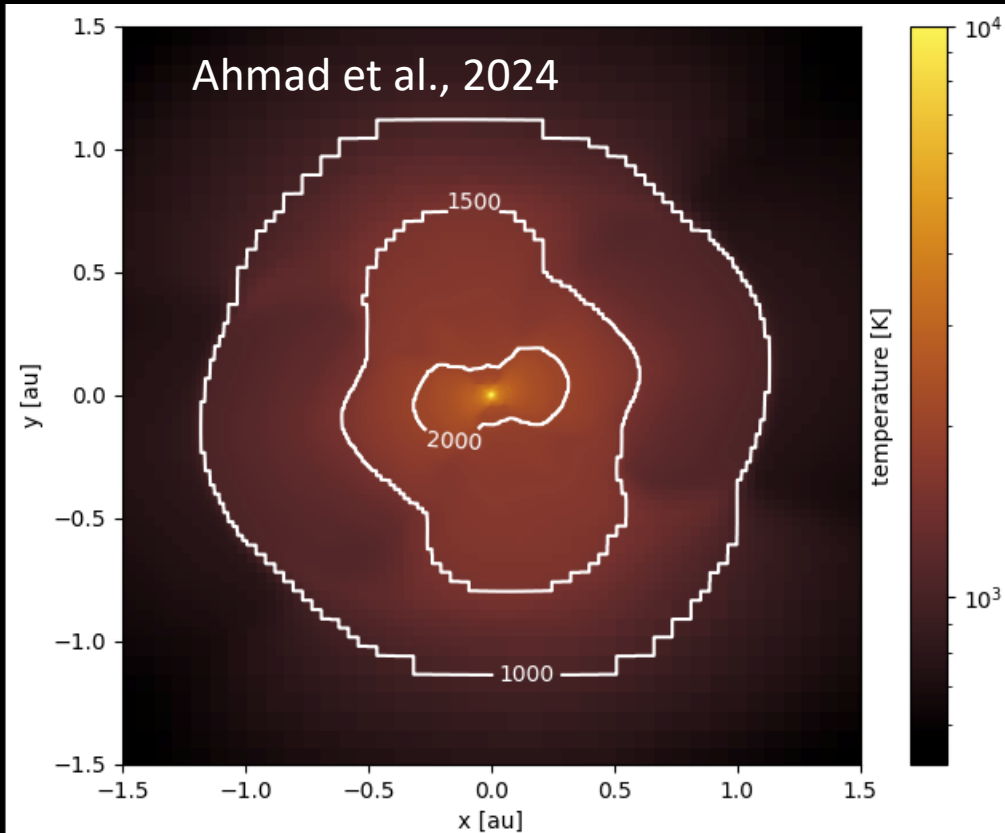
Fig. 6. The onset of condensation at $p = 1$ bar for solar abundances in phase equilibrium. The graph shows the concentration of the various condensed species with respect to hydrogen nuclei.



But « equilibrium » is maybe NOT a fully right assumption....

- CAls disappears at low temperature: => need 'isolation factor' (see Petaev et al.)
- Equil. : Does not tell WHAT reaction leads to equilibrium (=> just lowest Gibbs E.)

MHD collapse simulations show complex inflow structure & short timescales



Complex inflow structure

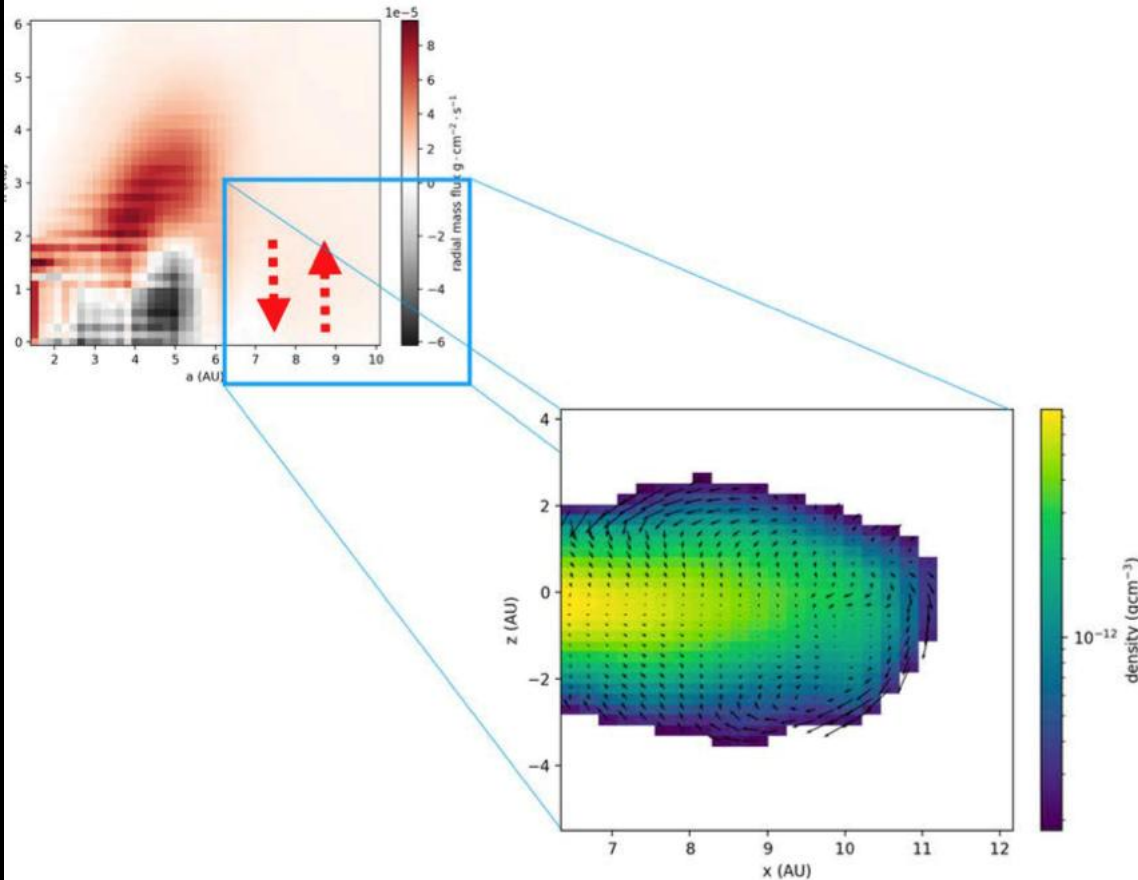


Fig. 13. Dynamics of gas as the envelope accretes onto the disk. It is obtained from the simulations described in [Commerçon et al. \(2024\)](#), after averaging over the elliptic motion of the gas streamlines around the star. The main plot shows the net radial flux, which is directed toward the star at the surface of the disk (red color) and outward near the midplane (gray color), whereas there is no net radial component beyond ~ 6 au, where instead the motion of the gas is vertical. The latter is illustrated by black arrows in the inlet, where the color depicts the density of gas.

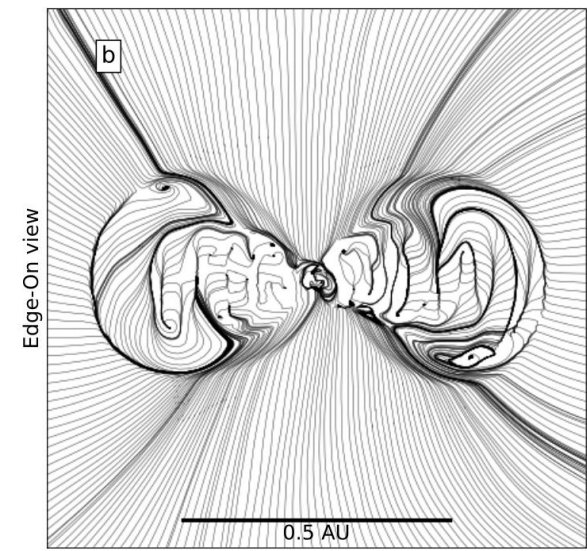


Fig. 5: Unbroken velocity vector field streamlines of run G1 at $t \approx 322$ days after the birth of the inner disk, illustrating the dynamics of accretion onto the disk and protostar in a top-down (panel a) and edge-on (panel b) view. The scale bar in panel (b) applies to panel (a) as well. An animated version of these streamlines, made using [windmap](#), is available in the online journal.

Ahmad et al., 2024

Rapid condensation of fine grained amoeboid olivine aggregates (Marrocchi et al., 2019)

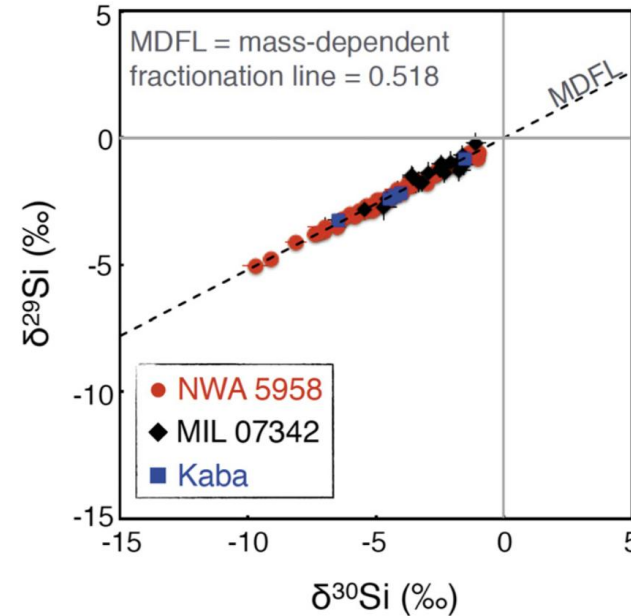
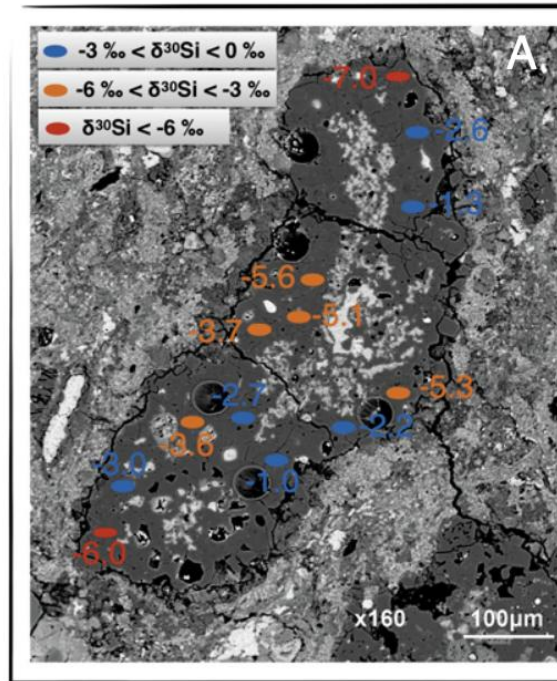


Fig. 2. Silicon 3-isotope plot showing the large range of mass-dependent isotopically light values measured in all analyzed AOAs in NWA 5958 (red), MIL 07342 (black), and Kaba (blue).

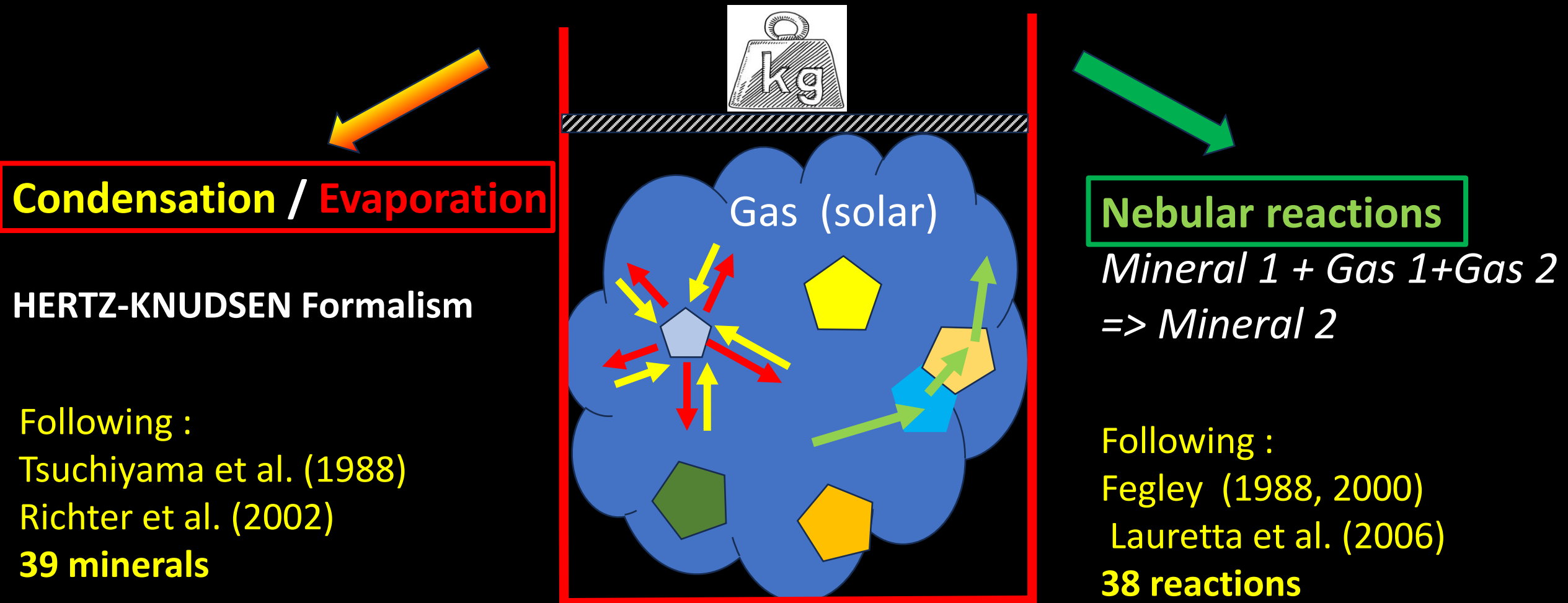
Fig. 1. A representative AOA and the Si isotopic compositions of its olivines. (A) Back-scattered electron image of AOA N1-8 from the CM-related chondrite NWA 5958 (30, 31). SIMS measurements are indicated by colored ellipses and the Si isotopic compositions associated with each analysis point. The color of the ellipses indicates the variability of the Si isotopic compositions by the range of the $\delta^{30}\text{Si}$ value: blue, $-3\text{‰} < \delta^{30}\text{Si} < 0\text{‰}$, orange, $-6\text{‰} < \delta^{30}\text{Si} < -3\text{‰}$, and red, $\delta^{30}\text{Si} < -6\text{‰}$. (B) $\delta^{29}\text{Si} - \delta^{30}\text{Si}$ diagram showing the mass-dependent variation observed in N1-8; MDFL, mass-dependent fractionation line.

Large mass dependant Si fractionation, light isotopes dominate=> condensation process

Condensation time : 10^5 seconds only (1-2 days !!!)

Kinetic condensation sequence ? How to calculate ?

Write all possible reactions...(well.. most important..)



Condensation evaporation in **Hydrogen** : Hertz Knudsen law

$$\frac{dN_{min}}{dt} = \overset{\text{Condensation}}{\gamma S \sum_{i,gas} \frac{P_{g,i}}{\sqrt{2\pi m_i kT}}} - \overset{\text{Evaporation}}{\gamma S \sum_{i,sat} \frac{P_{sat,i}}{\sqrt{2\pi m_i kT}}}$$

Richter et al. (2002, 2004, 2007) Fedkin et al. (2013)

$P_{g,i}$: partial pressures in the gas surrounding the mineral

$P_{sat,i}$ for every species. : saturating vapor pressure for every mineral

These value depend on the local chemistry of the gas, and in the abundance of H

One big unknown the « sticking coefficient » : The gamma term in the HZ equation

Our approach : We pre-compute evaporative flux (look-up tables)
we compute in real time condensation fluxes

→ $P_{i,sat,i}$ for every species. : Pre-Calculated by computing mineral-H₂ equilibrium

We use a chemical code (CEA/NASA) with mineral condensation to pré-calculate the $P_{ij,sat}$ for 38 minerals, in the presence of H

→ $P_{g,i}$: partial pressures in the gas surrounding the mineral
computed for the instantaneous composition of the gas

We assume local thermodynamical equilibrium of GAS

We use a chemical code (CEA/NASA) to compute the gas molecular species assuming

For all atoms in gas (H, O,C, Fe, Ni, Ca, Mg, Si, K, Cr..)

ASSUMPTIONS/SIMPLIFICATIONS:

(1) gas is at thermodynamic Equilibrium

(2) minerals contact surface is constant (no nucleation model)

Tabulated evaporation rate in H₂

Comparison with experiment (Tsuchiyama et al., 1998)

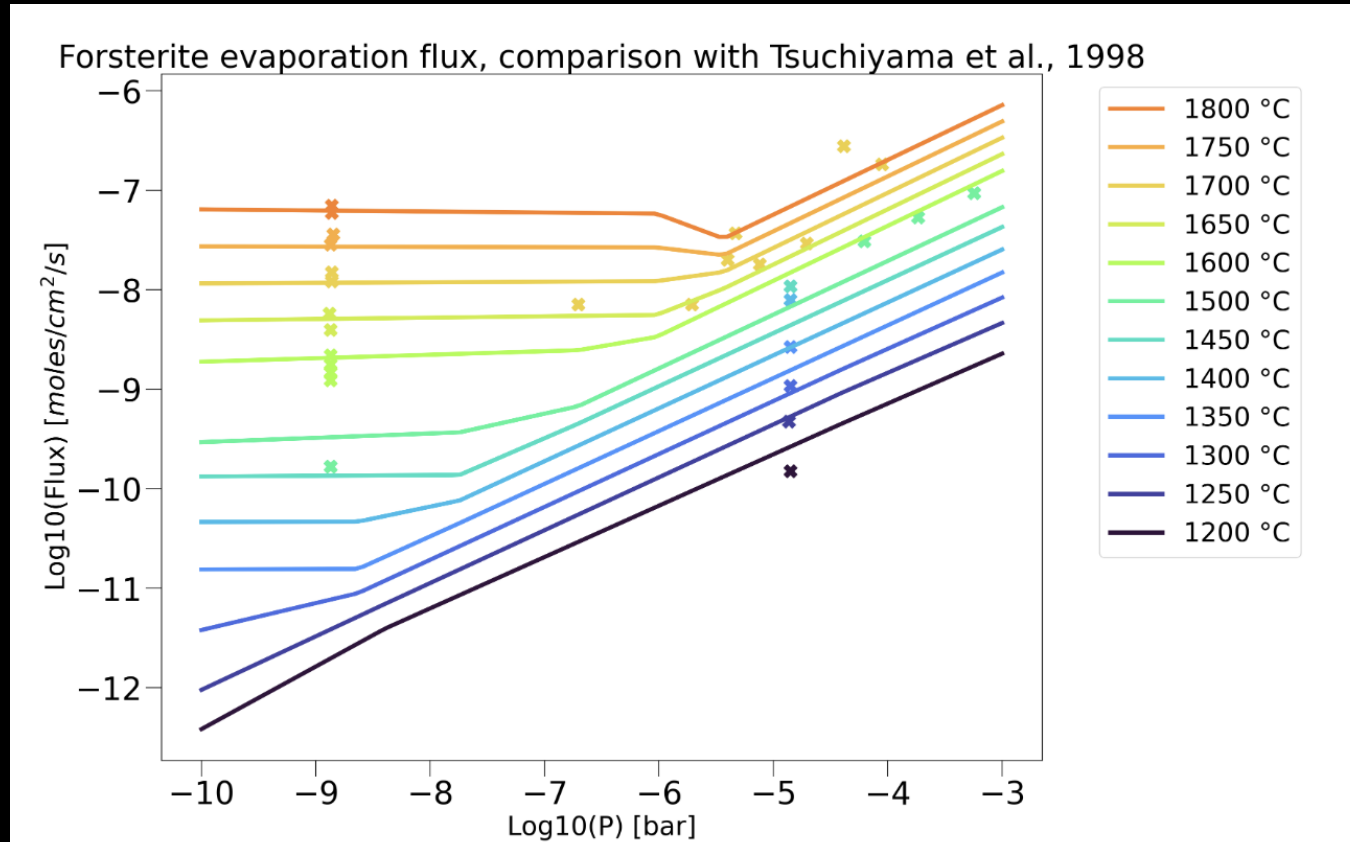
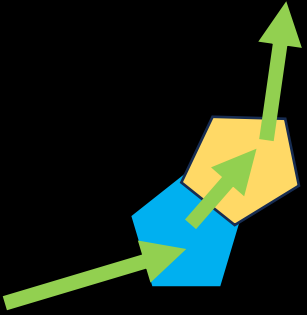


Fig. 1 Comparison of the Mg_2SiO_4 evaporation flux tabulated in KineCond (solid lines) and measured flux in laboratory experiments [3] (crosses). P is the total pressure of hydrogen species in the gas. At low hydrogen pressure, the vacuum evaporation flux is recovered, whereas at high hydrogen pressure, the effect of hydrogen increases the evaporative flux. Good match between the model and experimental data is observed.

Gas-mineral interactions : « nebular reactions »

One pre-existing mineral (M1) is transformed into another one (M2)



Many reactions... Simplest form :



The kinetics of these reactions depend on details of surface physics:

They depend on an activation energy

The most simplest case : The Simple Kinetic Theory (Fegley et al., 1999)

Mineral 1 + gas => Mineral 2

$$\frac{dN_2}{dt} = Flux(gas) * surface * e^{-Ea/RT}$$

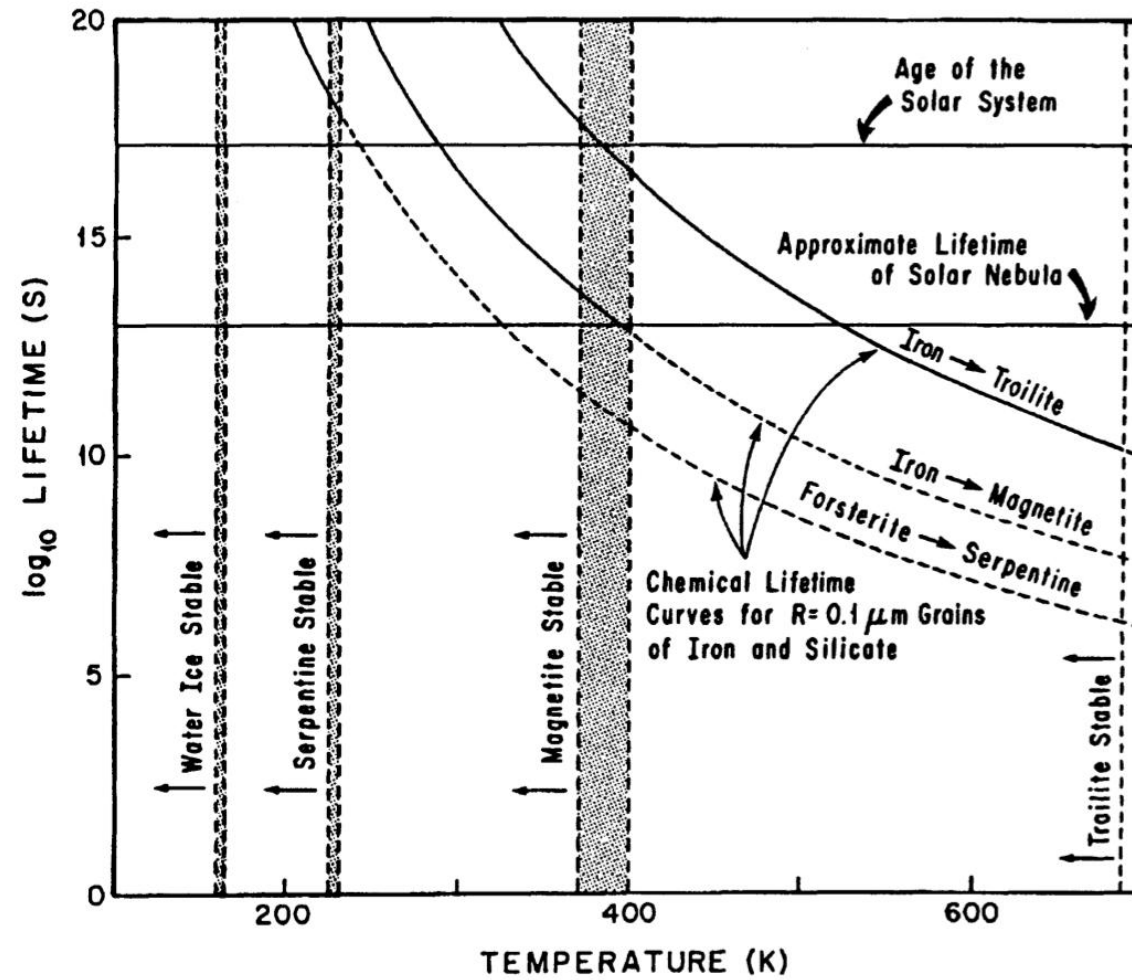
$Ea \sim 100 \text{ KJ/mol}$ for $\text{Fe} + \text{S} \Rightarrow \text{FeS}$ (Fegley et al., 1993)

\Rightarrow Iron can be sulfidized into FeS during Solar nebula life

Fegley et al., 1993 (at $T=700\text{K}$)

$Ea \sim 70 \text{ KJ/mol}$ for phyllosilicates or magnetite formation from

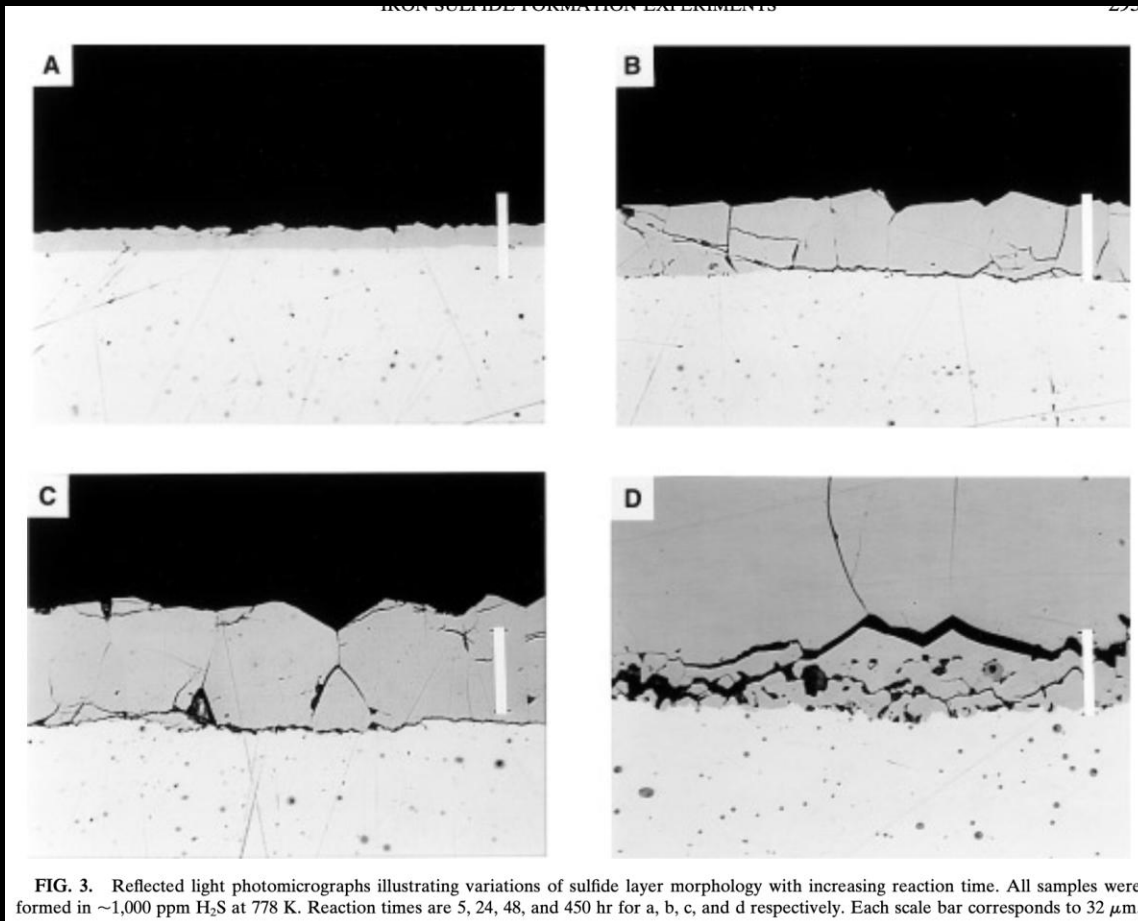
But $T < 400\text{K}$



Fegley et al. 1993

But this is a simple representation of gas-grains reactions.

Surface reactions are important and they are present in 2 regimes :
Linear and parabolic



Lauretta et al., 1996

Sulfidation of iron :



Transition from linear to Kinetic reactions

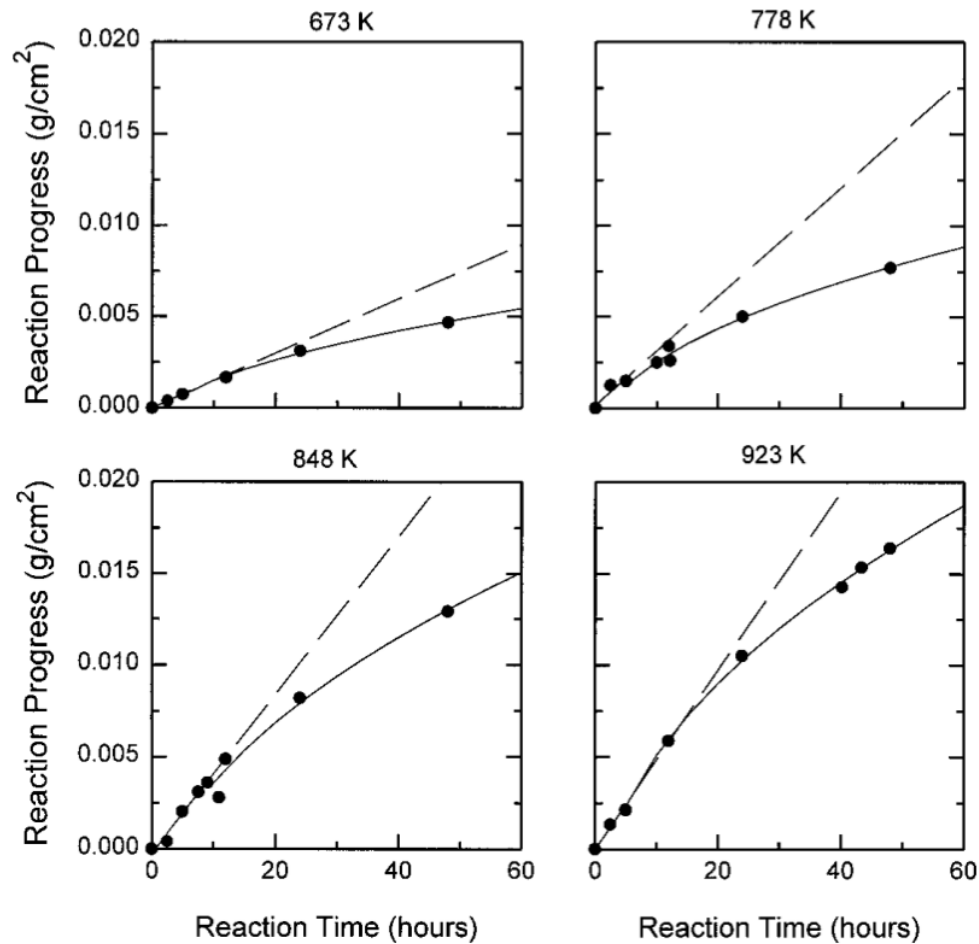


FIG. 15. Plots of reaction progress versus time along four isotherms (673, 778, 848, and 923 K) for samples formed in ~1,000 ppm H₂S. The dashed lines are linear least-squares fits to data points for experiments ≤10 hr. The solid curves are parabolic fits to longer reaction time experiments. Experiments at all temperatures show a transition from linear to parabolic kinetic behavior.

$$H \propto e^{-\frac{Ea_l}{RT}} \times t$$

The reaction rate is proportional to the flux of H₂S

$$H \propto e^{-\frac{Ea_p}{RT}} \times t^{\frac{1}{2}}$$

The reaction rate is controlled by the Diffusion of S inside the reaction layer

Comparison with experiments

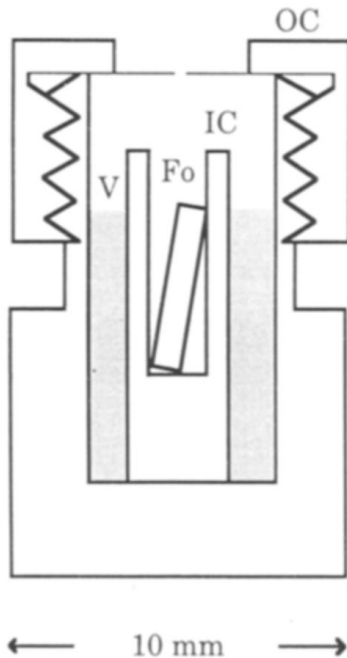


Fig. 1. Cross section of the double capsule. Outer capsule, with an orifice of 0.1 mm, acts as a Knudsen cell. OC = outer capsule (Mo); IC = inner capsule (Mo); Fo = single forsterite crystal ($1 \times 1.25 \times 5$ mm); V = cristobalite powder.

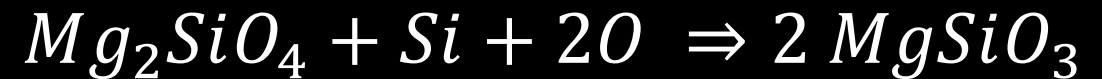
An experimental study of enstatite formation reaction between forsterite and Si-rich gas

Naoya Imae ^a, Akira Tsuchiyama ^b and Masao Kitamura ^a

^a Department of Geology and Mineralogy, Faculty of Science, Kyoto University, Kyoto 606, Japan

^b Institute of Earth and Planetary Sciences, College of Education, Osaka University, Toyonaka 560, Japan

Received October 13, 1992; revision accepted April 26, 1993



$$P \sim 10^{-7} \text{ bar}$$

Imae 1993

They found an activation energy in parabolic Regime : $\sim 500 \text{ KJ/mol}$

Comparison with experiments (Imae et al, 1993)

Growth of enstatite at the surface of a forsterite mineral

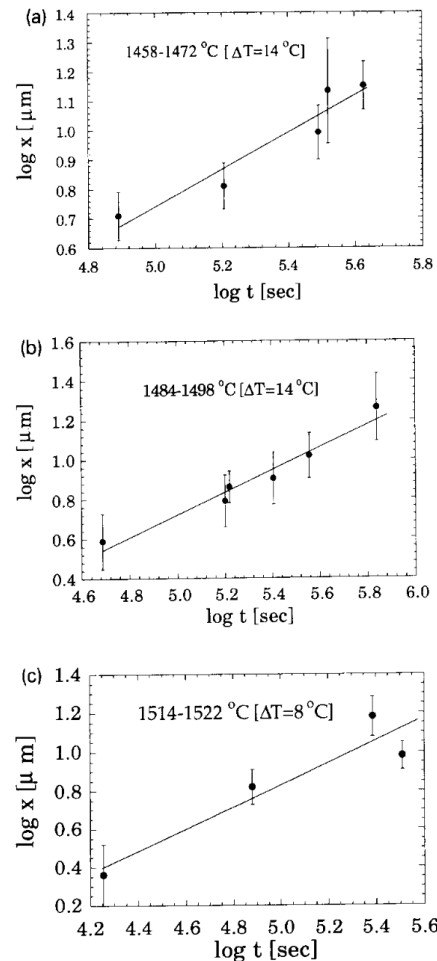


Fig. 4. Logarithm of enstatite width plotted against logarithm of time in nearly constant temperature ranges. (a) 1458–1472°C. (b) 1484–1498°C. (c) 1514–1522°C.

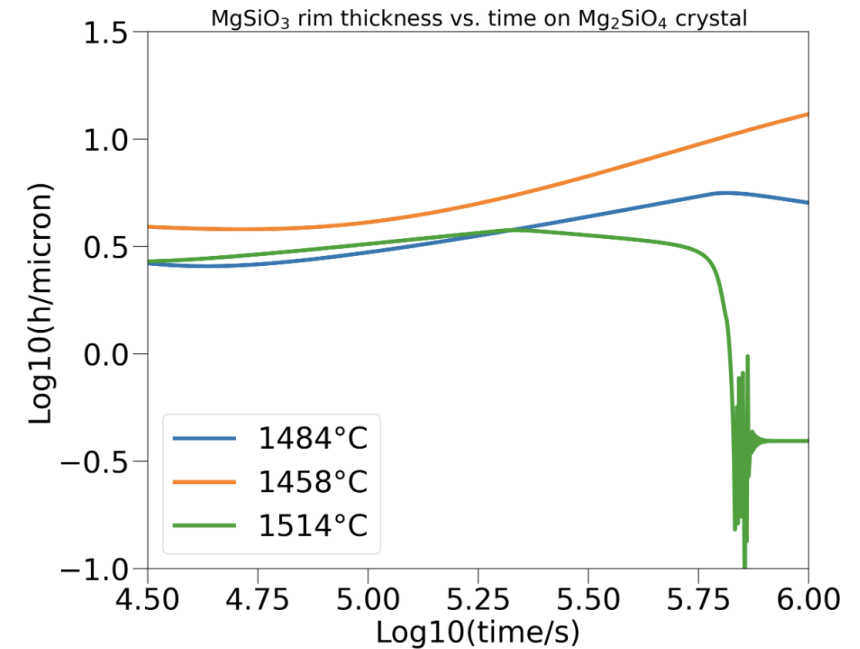


Fig. 2 Enstatite growth over a forsterite crystal in a SiO rich atmosphere, simulated with the KineCond code. Here the active rim thickness is plotted as a function of time for different temperatures. Compare with Figure 4 of [23]

Our simulation
(using E_a experimentally measured)

Only very few data exist for the activation energy of nebular reactions
In our code we will treat different members

We consider 3 cases

- Fast nebular reaction : (end member) $E_a^l = 0$ and $E_p^l = 0 \text{ KJ/mol}$
- Moderate nebular reaction : $E_a^l = 20 \text{ KJ/mol}$ and $E_p^l = 20 \text{ KJ/mol}$
- Slow nebular reactions : $E_a^l = 80 \text{ KJ/mol}$ and $E_a^p = 500 \text{ KJ/mol}$

Our choice of 38 (among about 50) REDUCED nebular reactions with the simple Mineral 1 + Gas 1 + Gas 2 => Mineral 2

Each reaction
Stands for
Many reaction
With same
Gas-grain exchanges.

1	$\text{Fe(s)} + \text{S} \rightarrow \text{FeS(s)}$
2	$\text{Fe(s)} + \text{O} \rightarrow \text{FeO(s)}$
3	$3 \text{FeO(s)} + \text{O} \rightarrow \text{Fe}_3\text{O}_4\text{(s)}$
4	$2 \text{FeO(s)} + \text{Si} + 2 \text{O} \rightarrow \text{Fe}_2\text{SiO}_4\text{(s)}$
5	$\text{Al}_2\text{O}_3\text{(s)} + 2 \text{Na} + \text{O} \rightarrow 2 \text{NaAlO}_2\text{(s)}$
6	$\text{NaAlO}_2\text{(s)} + 3 \text{Si} + 6 \text{O} \rightarrow \text{NaAlSi}_3\text{O}_8\text{(s)}$
7	$\text{NaAlO}_2\text{(s)} + 2 \text{Si} + 4 \text{O} \rightarrow \text{NaAlSi}_2\text{O}_6\text{(s)}$
8	$\text{Na}_2\text{O(s)} + 2 \text{Al} + 3 \text{O} \rightarrow 2 \text{NaAlO}_2\text{(s)}$
9	$\text{CaAl}_{12}\text{O}_{19}\text{(s)} + 2 \text{Ca} + 2 \text{O} \rightarrow 3 \text{CaAl}_4\text{O}_7\text{(s)}$
10	$2 \text{Al}_2\text{O}_3\text{(s)} + \text{O} + \text{Ca} \rightarrow \text{CaAl}_4\text{O}_7\text{(s)}$
11	$\text{Al}_2\text{O}_3\text{(s)} + \text{O} + \text{Ca} \rightarrow \text{CaAl}_2\text{O}_4\text{(s)}$
12	$\text{Al}_2\text{O}_3\text{(s)} + \text{O} + \text{Mg} \rightarrow \text{MgAl}_2\text{O}_4\text{(s)}$
13	$\text{CaAl}_2\text{O}_4\text{(s)} + 2 \text{Al} + 3 \text{O} \rightarrow 1 \text{CaAl}_4\text{O}_7\text{(s)}$
14	$\text{CaAl}_4\text{O}_7\text{(s)} + 8 \text{Al} + 12 \text{O} \rightarrow \text{CaAl}_{12}\text{O}_{19}\text{(s)}$
15	$6 \text{Al}_2\text{O}_3\text{(s)} + \text{O} + \text{Ca} \rightarrow \text{CaAl}_{12}\text{O}_{19}\text{(s)}$
16	$\text{Mg}_2\text{SiO}_4\text{(s)} + \text{Si} + 2 \text{O} \rightarrow 2 \text{MgSiO}_3\text{(s)}$
x 17	$\text{MgSiO}_3\text{(s)} + \text{Mg} + \text{O} \rightarrow \text{Mg}_2\text{SiO}_4\text{(s)}$
18	$\text{SiO}_2\text{(s)} + 2 \text{Mg} + 2 \text{O} \rightarrow \text{Mg}_2\text{SiO}_4\text{(s)}$
19	$\text{SiO}_2\text{(s)} + 1 \text{Mg} + \text{O} \rightarrow \text{MgSiO}_3\text{(s)}$
20	$2 \text{SiO}_2\text{(s)} + 2 \text{K} + \text{O} \rightarrow \text{K}_2\text{Si}_2\text{O}_5\text{(s)}$
21	$\text{SiO}_2\text{(s)} + \text{Ca} + \text{O} \rightarrow \text{CaSiO}_3\text{(s)}$
22	$\text{SiO}_2\text{(s)} + 2 \text{Fe} + 2 \text{O} \rightarrow \text{Fe}_2\text{SiO}_4\text{(s)}$
23	$\text{SiO}_2\text{(s)} + 2 \text{Ca} + 2 \text{O} \rightarrow \text{Ca}_2\text{SiO}_4\text{(s)}$
24	$\text{CaAl}_4\text{O}_7\text{(s)} + \text{Ca} + \text{O} \rightarrow 2 \text{CaAl}_2\text{O}_4\text{(s)}$
25	$\text{CaAl}_4\text{O}_7\text{(s)} + 8 \text{Al} + 12 \text{O} \rightarrow \text{CaAl}_{12}\text{O}_{19}\text{(s)}$
26	$\text{CaAl}_2\text{O}_4\text{(s)} + 2 \text{Al} + 3 \text{O} \rightarrow \text{CaAl}_4\text{O}_7\text{(s)}$
27	$\text{CaAl}_2\text{O}_4\text{(s)} + 2 \text{Si} + 4 \text{O} \rightarrow \text{CaAl}_2\text{Si}_2\text{O}_8\text{(s)}$
28	$\text{CaAl}_2\text{O}_4\text{(s)} + 10 \text{Al} + 15 \text{O} \rightarrow \text{CaAl}_{12}\text{O}_{19}\text{(s)}$
29	$\text{Ca}_2\text{SiO}_4\text{(s)} + 2 \text{Al} + 3 \text{O} \rightarrow \text{Ca}_2\text{Al}_2\text{SiO}_7\text{(s)}$
30	$\text{Ca}_2\text{SiO}_4\text{(s)} + \text{Si} + 2 \text{O} \rightarrow 2 \text{CaSiO}_3\text{(s)}$
31	$\text{Mg}_2\text{SiO}_4\text{(s)} + 2 \text{Ca} + 3 \text{Si} + 8 \text{O} \rightarrow 2 \text{CaMgSi}_2\text{O}_6\text{(s)}$
32	$\text{Mg}_2\text{SiO}_4\text{(s)} + 4 \text{Ca} + 3 \text{Si} + 10 \text{O} \rightarrow 2 \text{Ca}_2\text{MgSi}_2\text{O}_7\text{(s)}$
33	$\text{Al}_2\text{O}_3\text{(s)} + \text{Mg} + \text{O} \rightarrow \text{MgAl}_2\text{O}_4\text{(s)}$
34	$\text{MgSiO}_3\text{(s)} + \text{Ca} + \text{Si} + 3 \text{O} \rightarrow \text{CaMgSi}_2\text{O}_6\text{(s)}$
35	$\text{CaSiO}_3\text{(s)} + \text{Mg} + \text{Si} + 3 \text{O} \rightarrow \text{CaMgSi}_2\text{O}_6\text{(s)}$
36	$\text{Ca}_2\text{MgSi}_2\text{O}_7\text{(s)} + \text{Mg} + 2 \text{Si} + 5 \text{O} \rightarrow 2 \text{CaMgSi}_2\text{O}_6\text{(s)}$
37	$\text{NaAlO}_2\text{(s)} + \text{Si} + 2 \text{O} \rightarrow 1 \text{NaAlSiO}_4\text{(s)}$
38	$3 \text{Fe(s)} + 4 \text{O} \rightarrow \text{Fe}_3\text{O}_4\text{(s)}$

Charnoz et al., 2024

Results

1) Close-to equilibrium condensation (high pressure, long cooling time)

1) out-of-equilibrium condensation (low pressure, short cooling time)

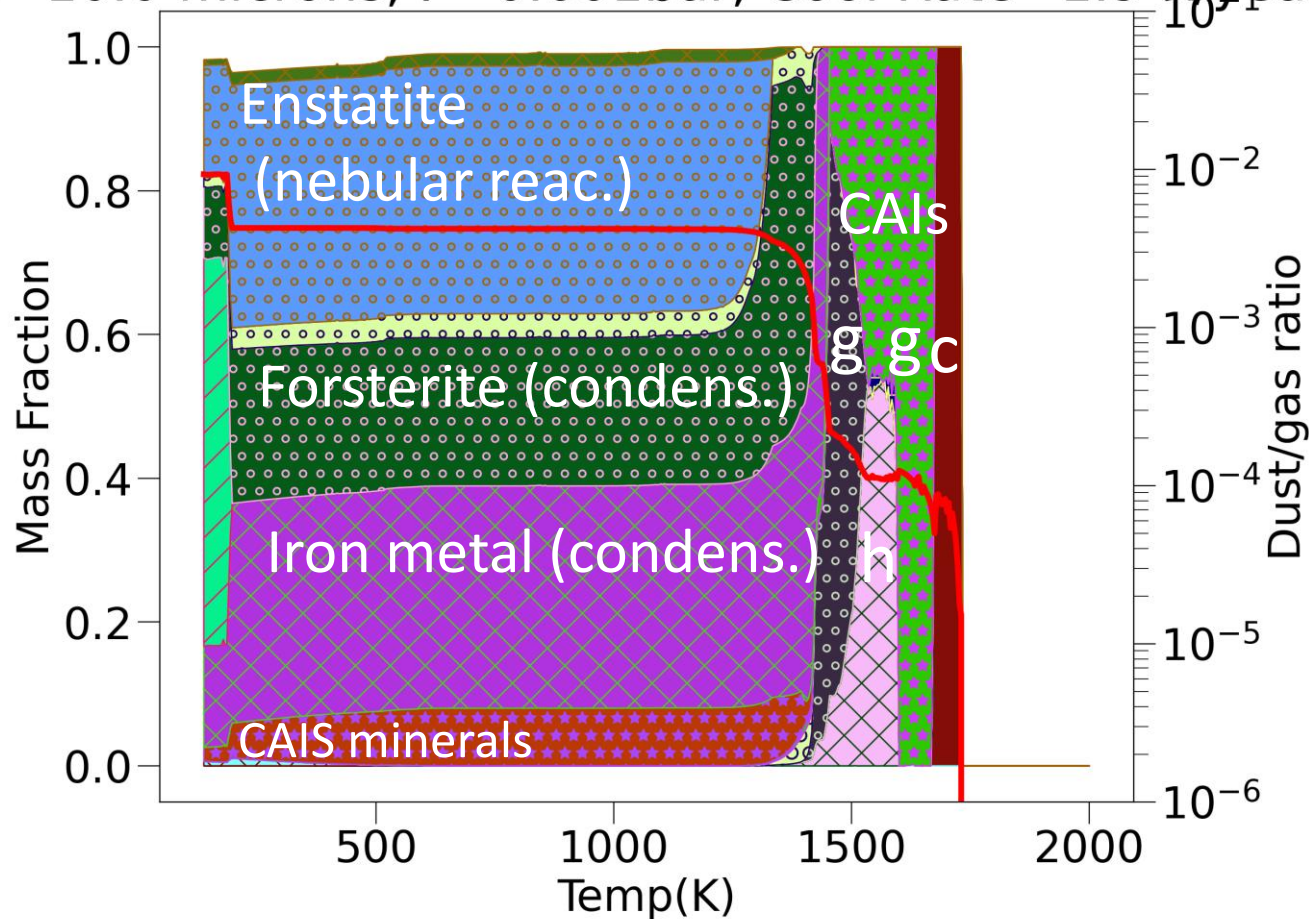
Condensing slowly (1000 yrs) and at high pressure (10^{-3} bar)

Do we recover « equilibrium » condensation sequence on long time ?

Yes + we preserve CAIs at low temperature

Kinetic (fast nebular interactions)

R=10.0 microns, P=0.001bar, Cool Rate=1.9 K/year

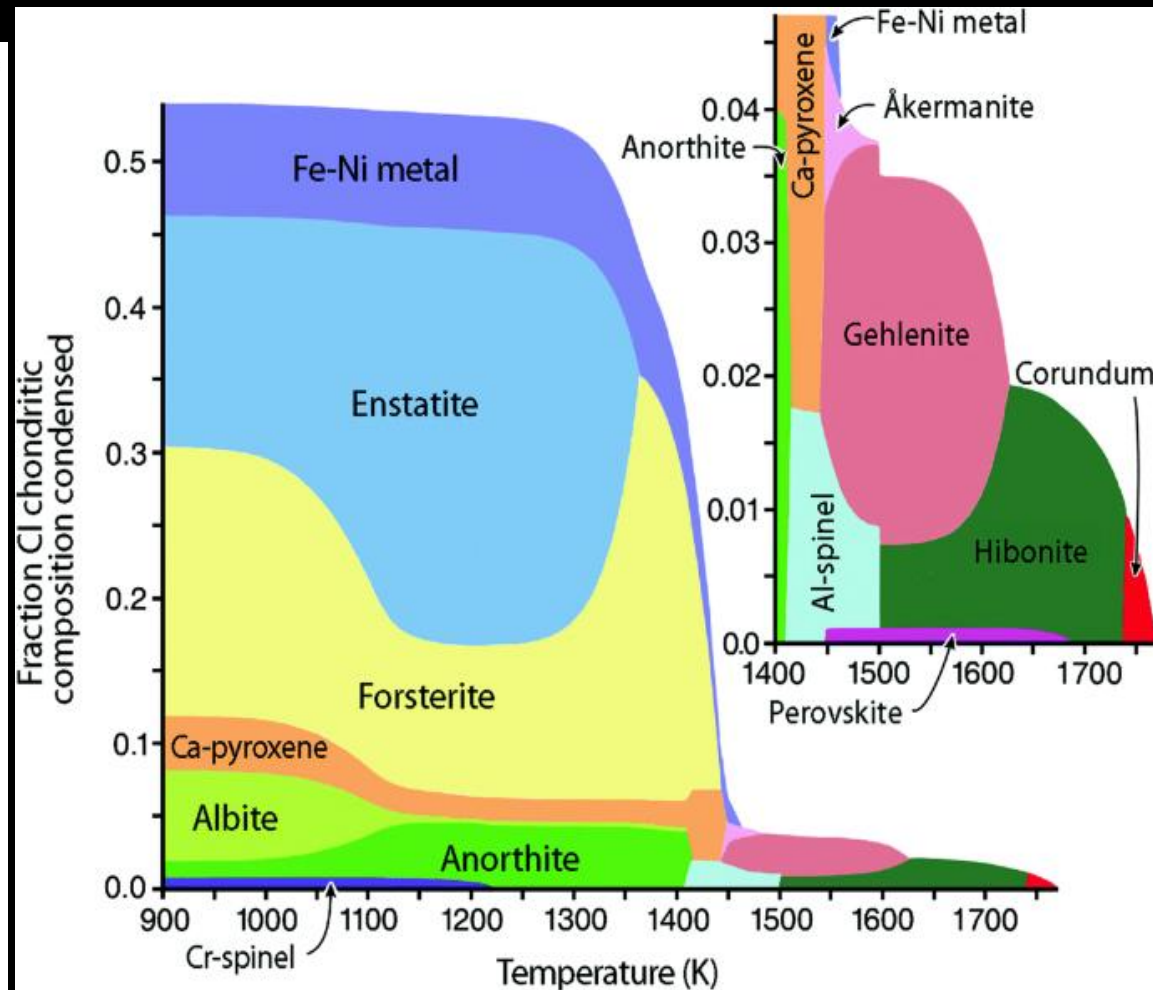
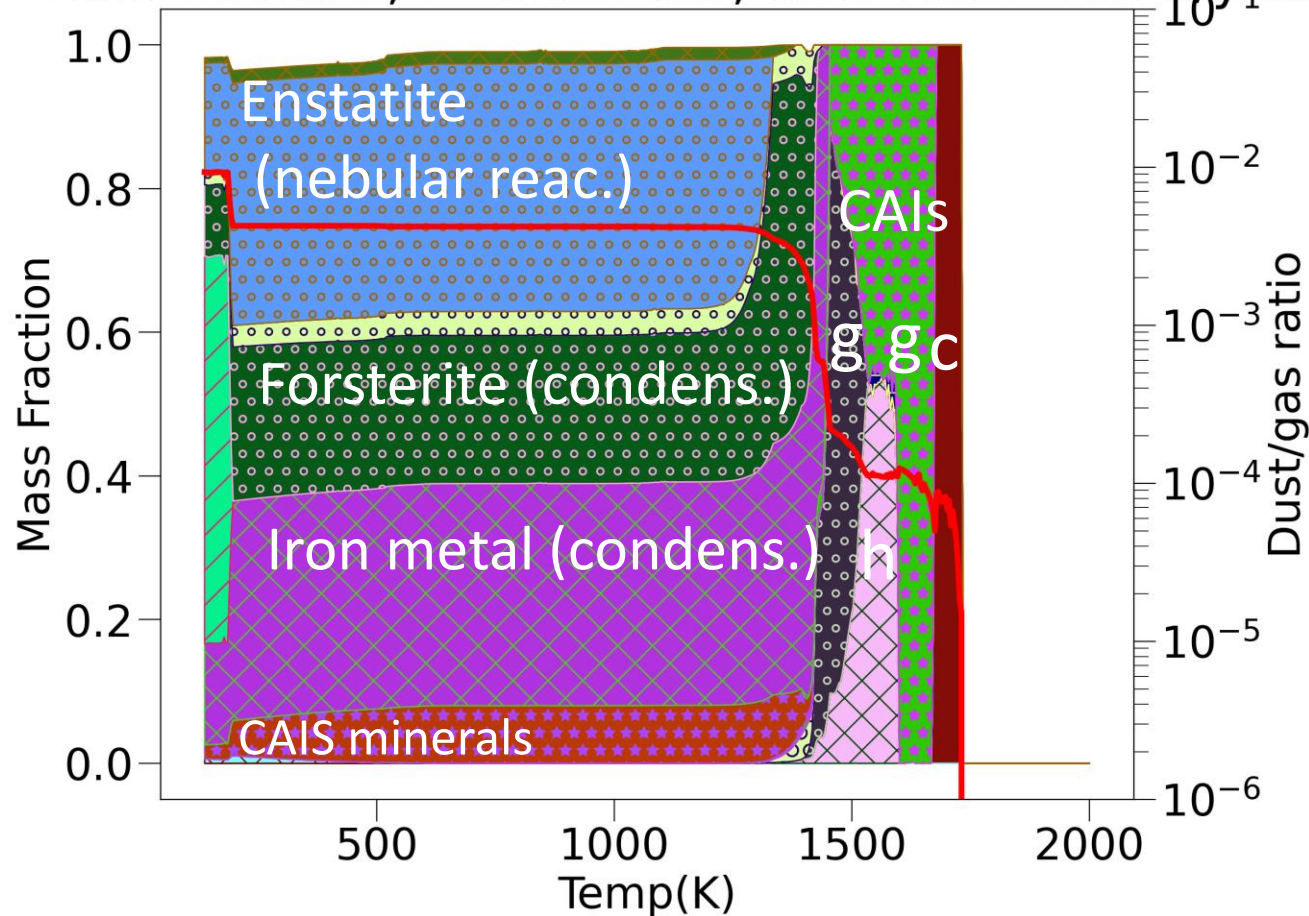


	Al ₂ O ₃ (cr), Corun
	Ca ₁ Al ₁₂ O ₁₉ (cr), Hibon
	Ca ₁ Si ₁ O ₃ (cr), Wolla
	Ca ₂ Al ₂ SiO ₇ (cr), Ghele
	Ca ₂ MgSi ₂ O ₇ (cr), Akerm
	CaAl ₂ O ₄ (cr), Kroti
	CaAl ₄ O ₇ (cr), Gross
	CaMgSi ₂ O ₆ (cr), Diops
	Fe(cr), Iron
	H ₂ O(cr), Water
	Mg ₂ SiO ₄ (cr), Forst
	MgAl ₂ O ₄ (cr), Spine
	MgSiO ₃ (cr), Ensta
	Ni(cr), Ni1

Comparison with classical equilibrium condensation sequence Obtained by Gibbs Energy minimisation ($P=10^{-3}$ bar)

Yoneda & Grossman 1972

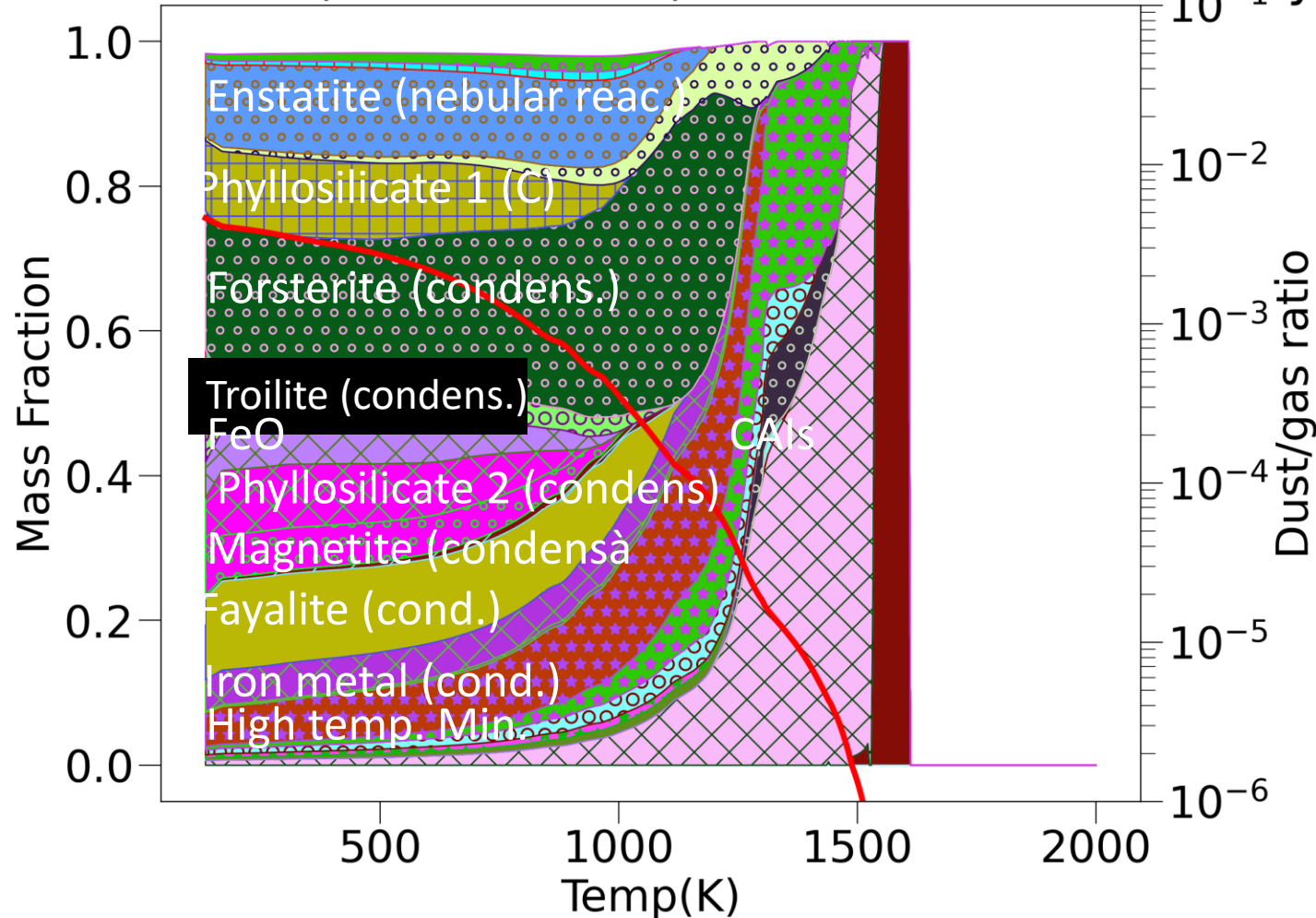
$R=10.0$ microns, $P=0.001$ bar, Cool Rate= 1.9 K/year



Condensing rapidly (10yrs) and at low pressure(10^{-7} bar) : surprises !

Either rapid or slow nebular reactions=>

R=10.0 microns, P=1e-05bar, Cool Rate=19000.0 K/year



rich diversity of minerals



Formation of oxidized phases :
Fayalite,
phyllosilicates, magnetite etc..



**Final mineralogy « apparently »
oxidized... without
more water nor O₂ !**

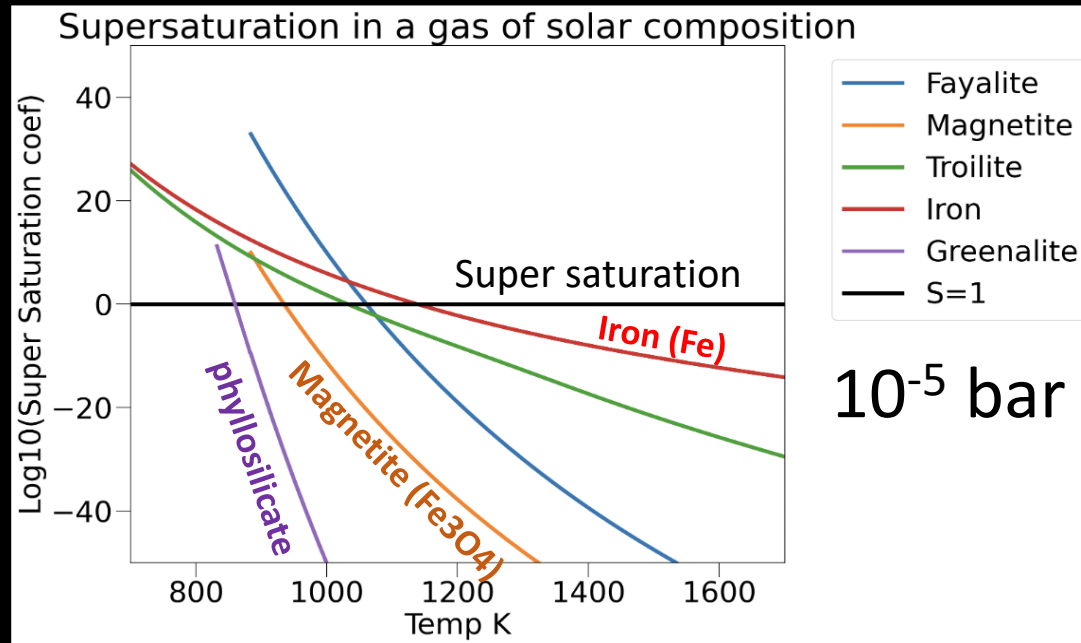
What happens in low pressure/fast cooling ?



Major elements in the gas (Si, Al, Fe..) have no time to condense in fast cooling at high temp.



They become available to react at low temperature where oxides become super-saturated

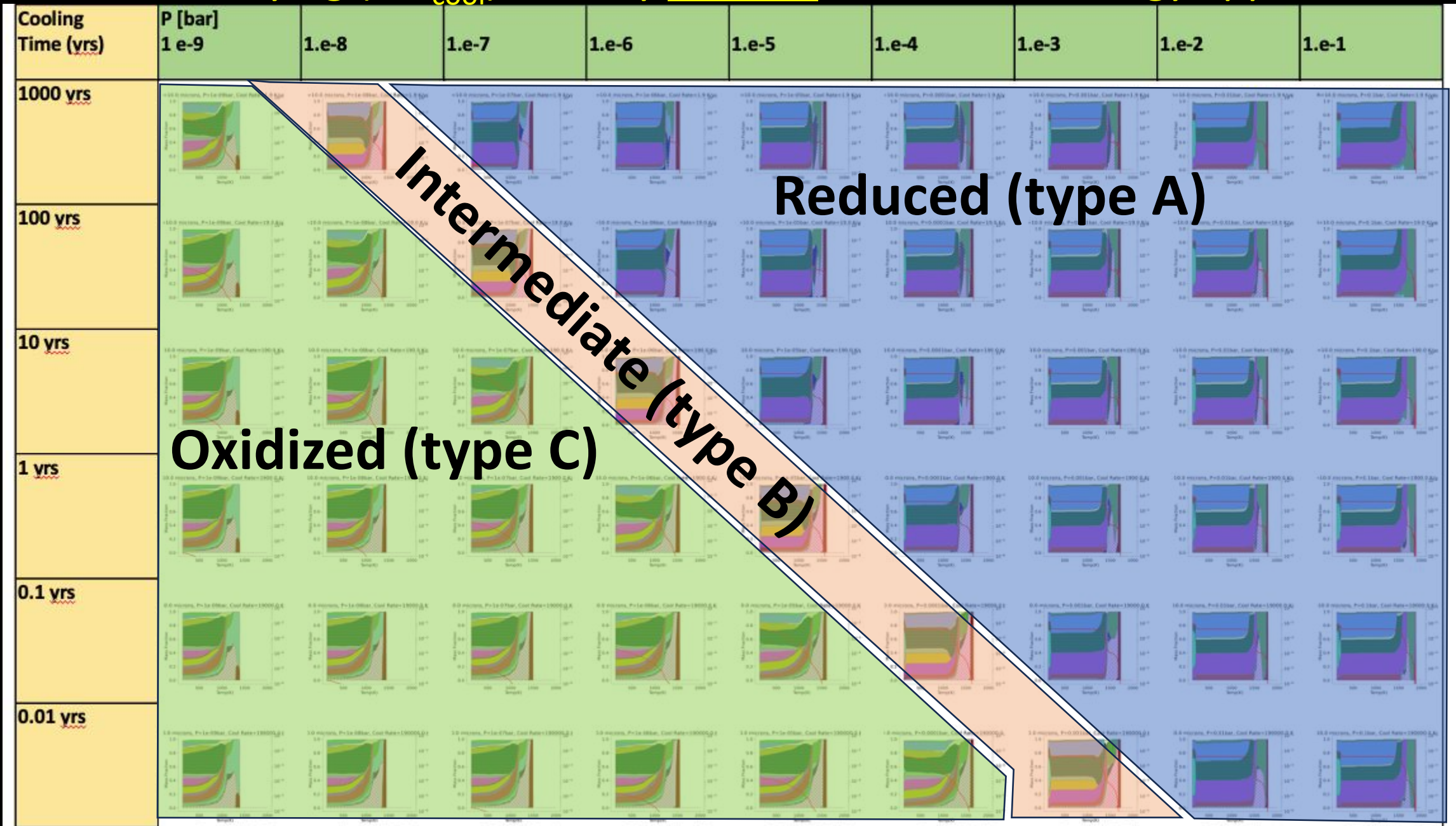


Systematic exploration of P and Tc : cooling time

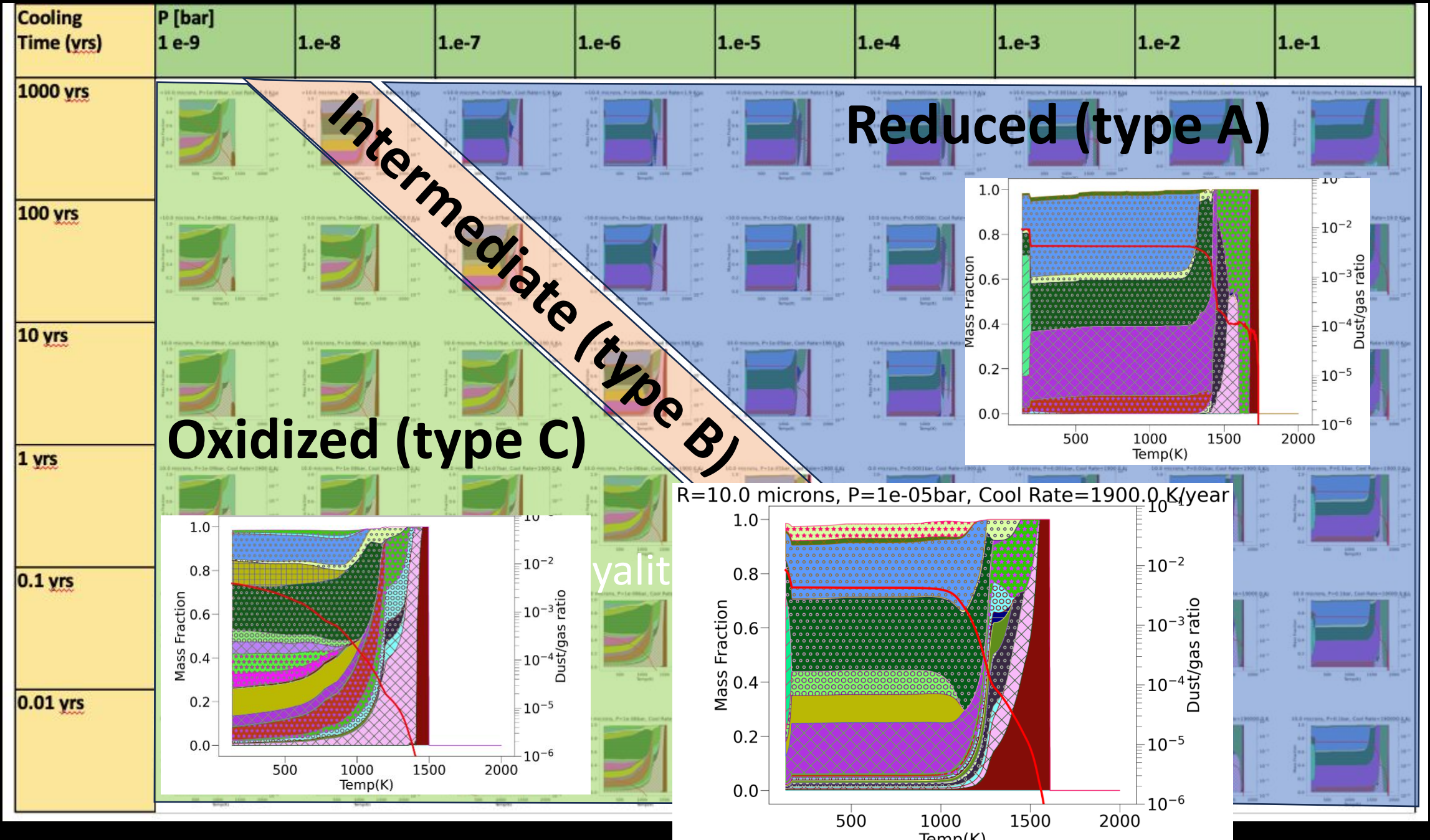
when varying $(P, T_{\text{cool}}) \Rightarrow$ Only 3 types of dust mineralogy appear

Cooling Time (yrs)	P [bar] 1 e-9	1.e-8	1.e-7	1.e-6	1.e-5	1.e-4	1.e-3	1.e-2	1.e-1
1000 yrs									
100 yrs									
10 yrs									
1 yrs									
0.1 yrs									
0.01 yrs									

when varying (P, T_{cool}) => Only 3 types of dust mineralogy appear



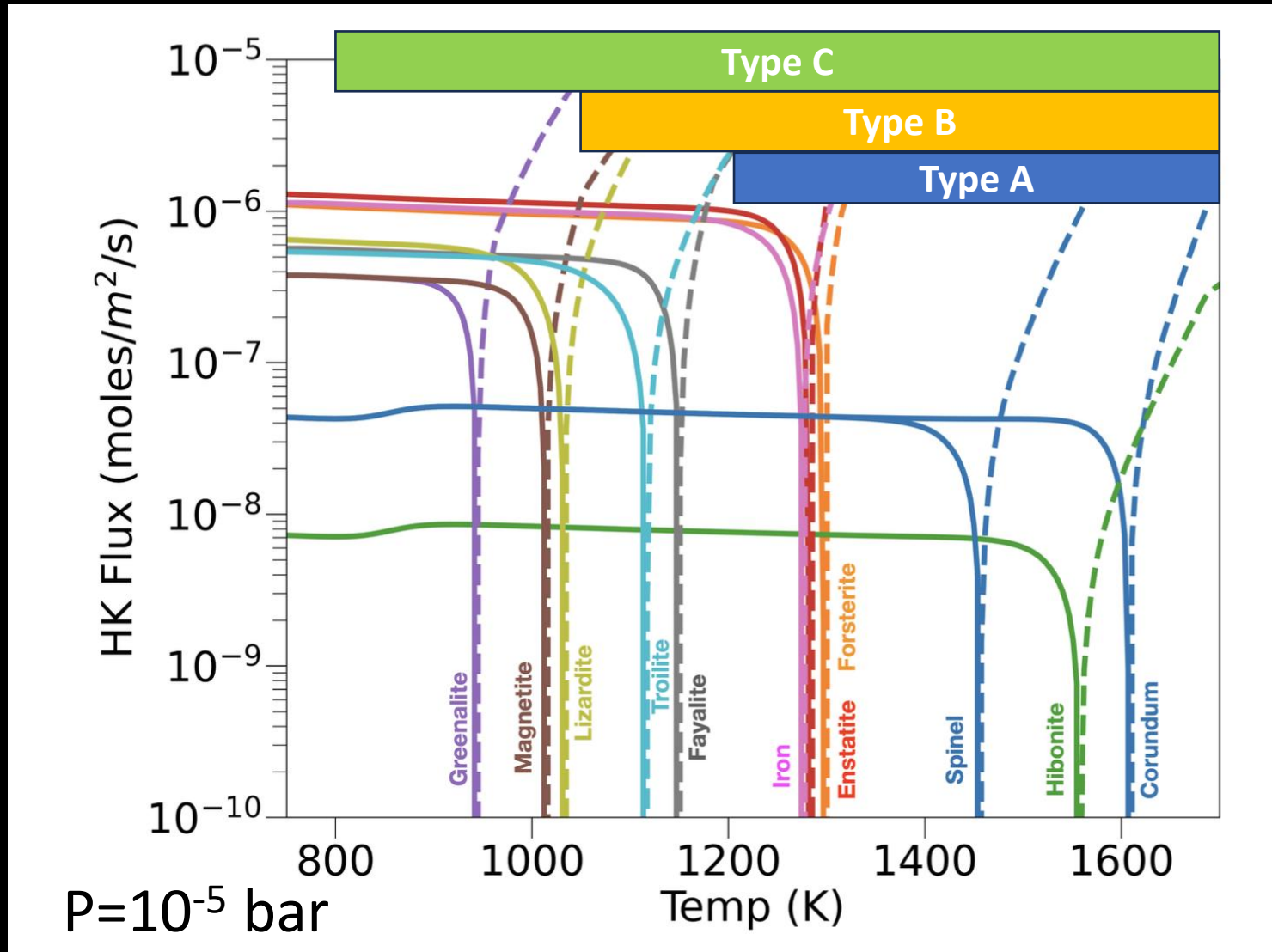
Only 3 types of dust mineralogy appear (when varying (P, T_{cool}))



Why 3 discontinuous classes of mineralogies ?

=> Fast temperature drop allows to condense lower temperature minerals (if condensation is incomplete)

Hertz Knudsen Fluxes



Reduced (A):

All atoms condensed above 1200K
(slow cooling)

slightly oxid. (B):

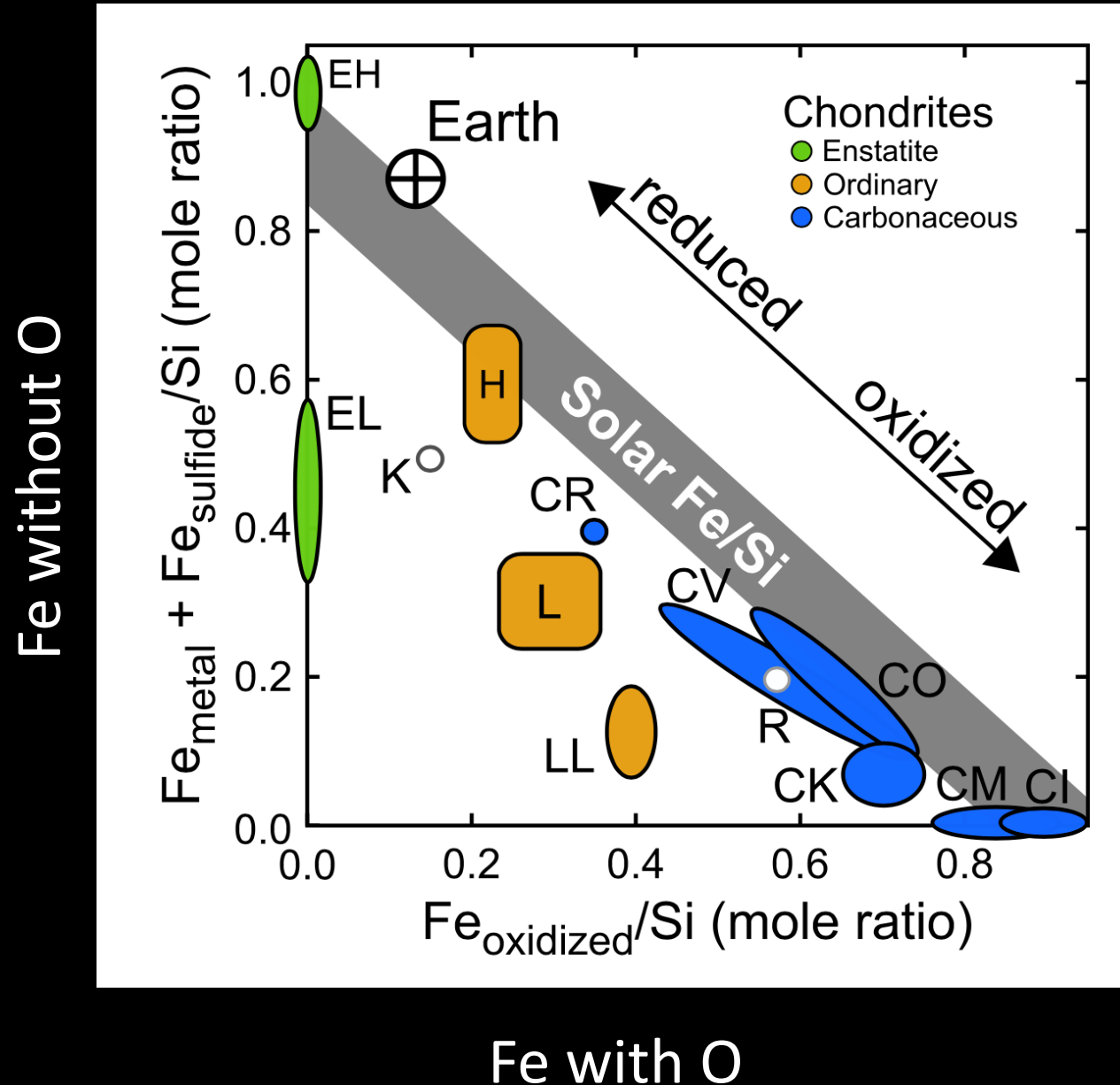
All atoms condensed above 1100K
Contains **Fayalite + Fe metal**
(quite fast cooling)

Very oxidized(C):

Most atoms condensed below 800K
Contains Fayalite, phyllos., magnet., etc.
(very fast cooling)

Computing oxydation level and
Evolution in the Urey-Craig Diagram Oxidation diagram

The Urey-Craig Diagram (1953) : a proxy for the oxidation state of chondrites



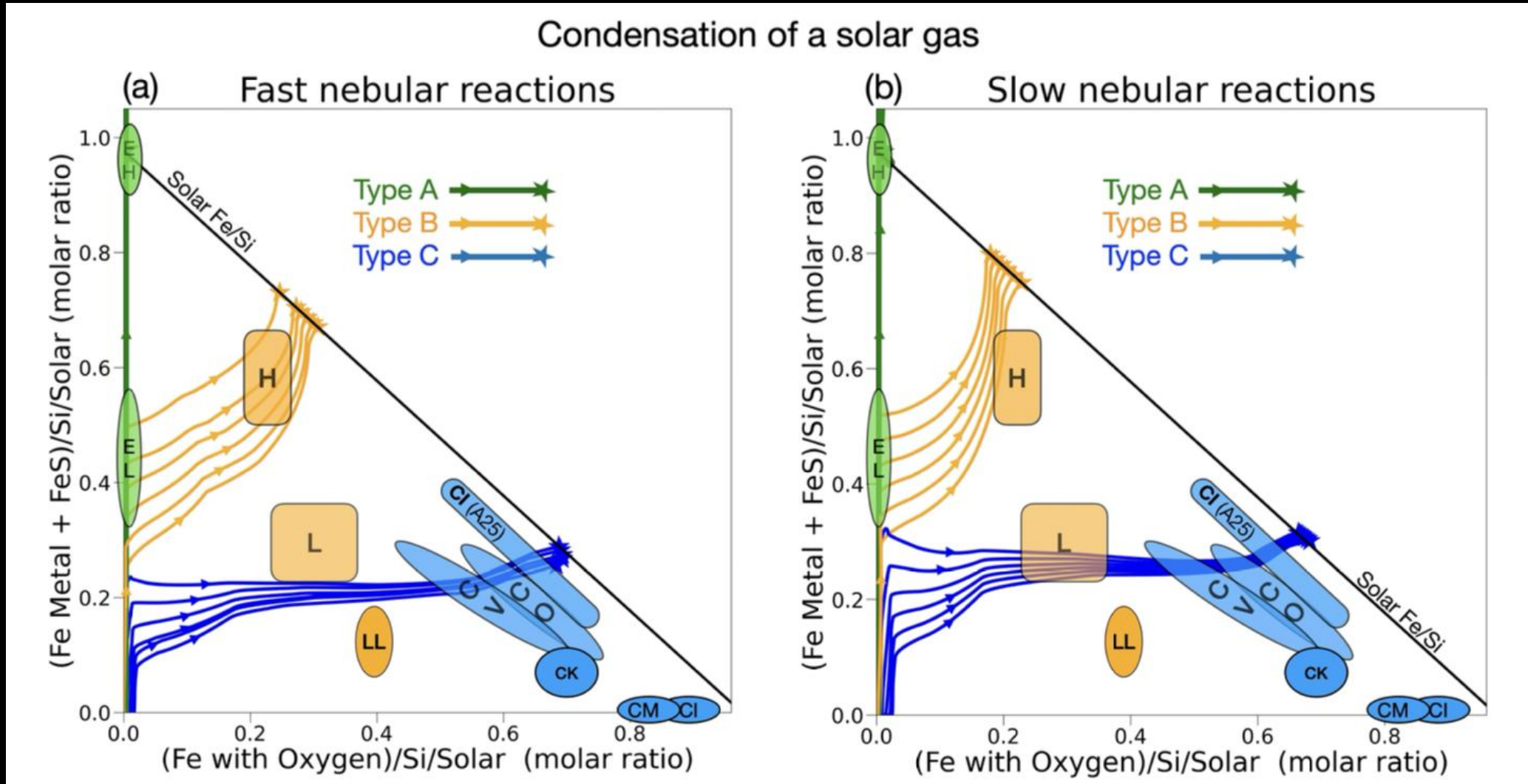
(Urey & Craig, 1953)
adapted from
Yoshizaki et al. (2021)

- Discontinuous mineralogies

Recovering the « classical » Iron Oxidation Diagram (Urey Craig)

Rapid nebular reactions

Slow nebular reactions



Discontinuous mineralogies : nothing between the 3 classes

For Fast cooling => kinetic of nebular reactions play a minor role=> **Condensation dominates**

Computing Equivalent fO_2

What would be the apparent fO_2 of the Mineral assemblage we calculated ?

Re-equilibrating our mineralogies with FACTSAGE

Apparent fo2 of mineral assemblage

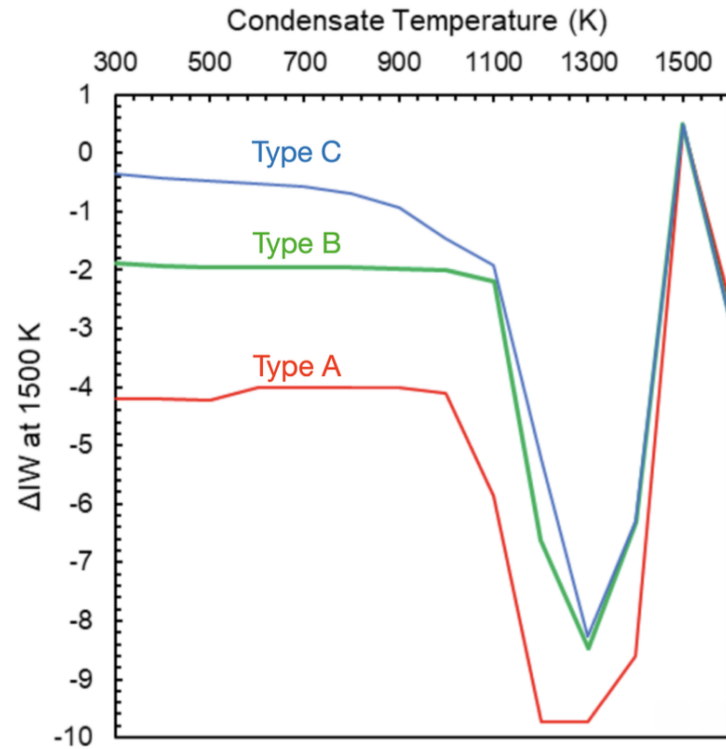
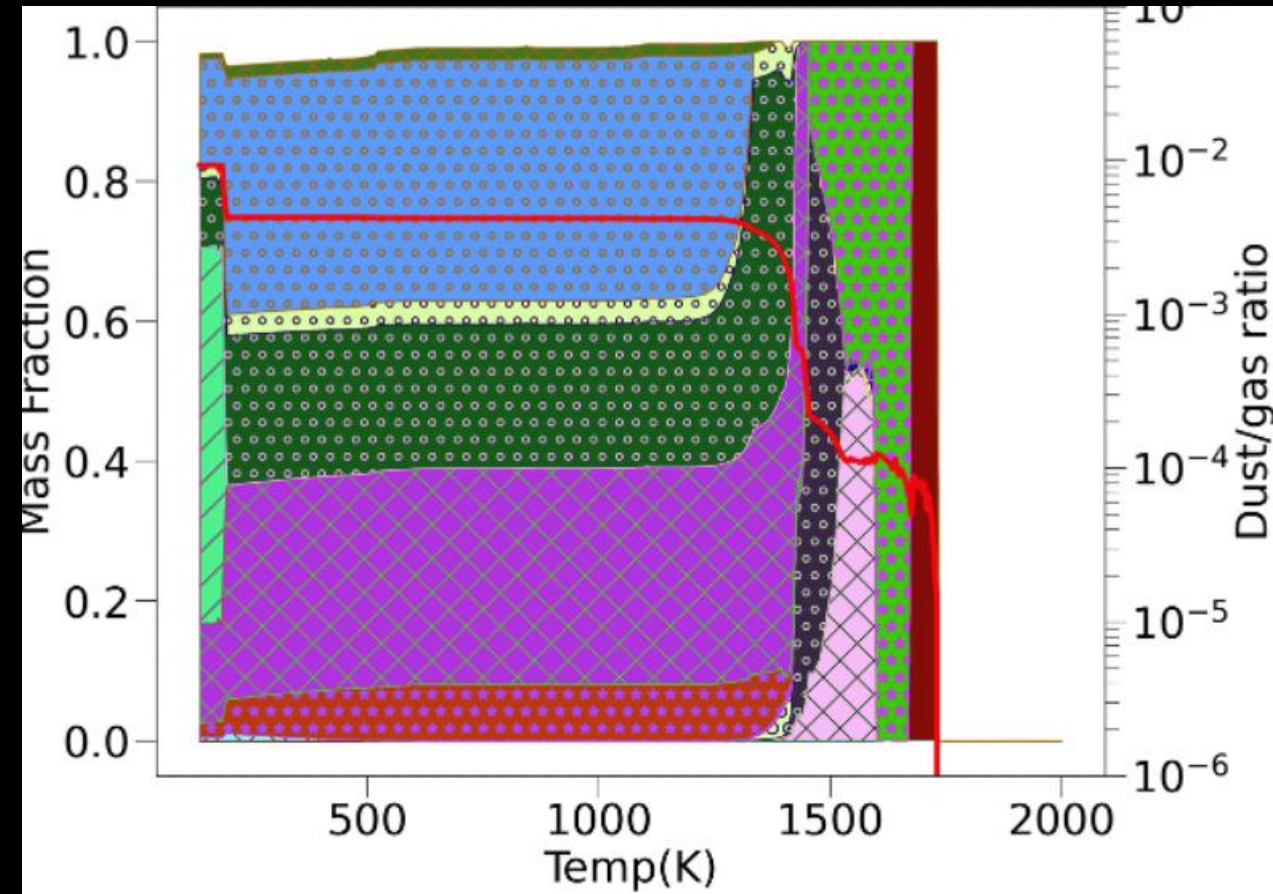


Fig. 14 Equivalent f_{O_2} of re-equilibrated mineralogies for the three types A,B and C. The X axis stands for the temperature at which condensates are considered, while the Y axis gives the equivalent f_{O_2} (with respect to the iron-wustite buffer). Here the types A,B,C are computed using the fast nebular reaction case.

Type A



Re-equilibrating our mineralogies with FACTSAGE

Apparent fo2 of mineral assemblage

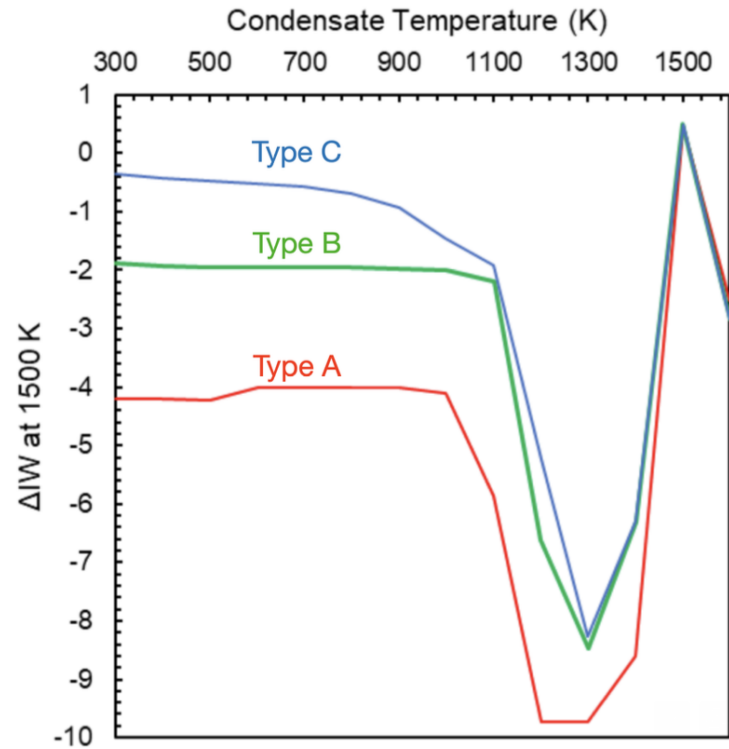
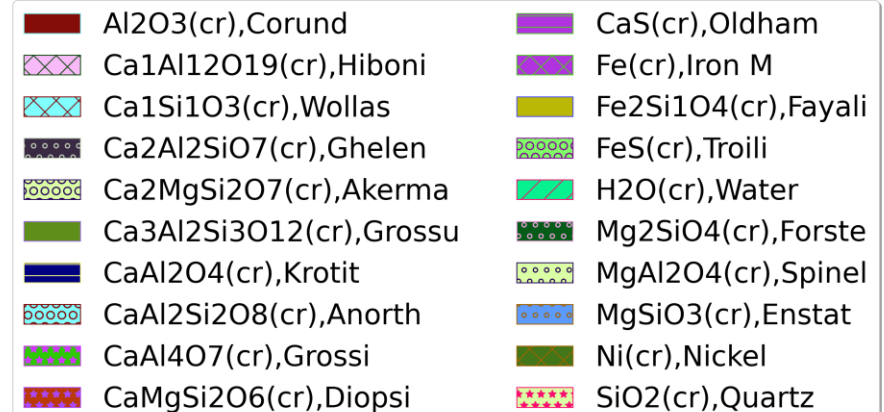
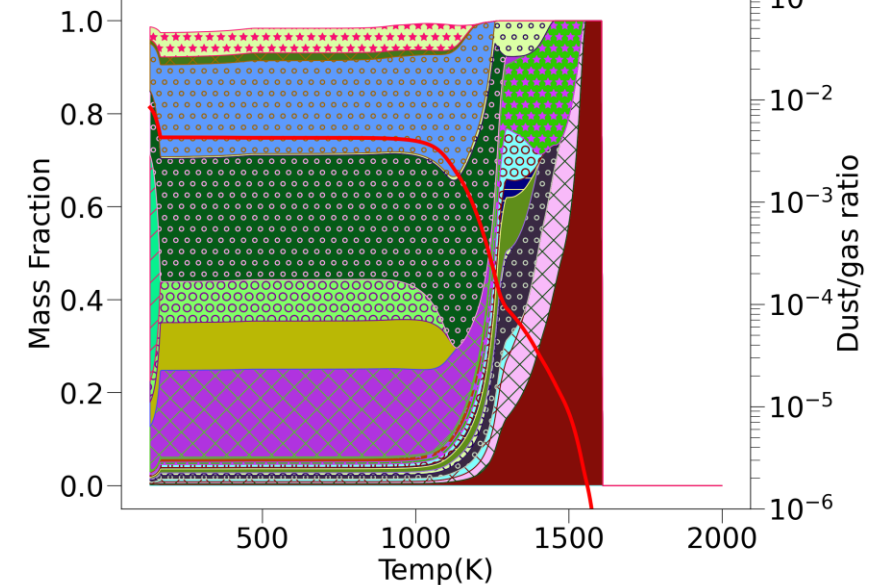


Fig. 14 Equivalent f_{O_2} of re-equilibrated mineralogies for the three types A,B and C. The X axis stands for the temperature at which condensates are considered, while the Y axis gives the equivalent f_{O_2} (with respect to the iron-wustite buffer). Here the types A,B,C are computed using the fast nebular reaction case.

Type B

R=10.0 microns, P=1e-05bar, Cool Rate=1900.0 K/year



Re-equilibrating our mineralogies with FACTSAGE

Apparent fo2 of mineral assemblage

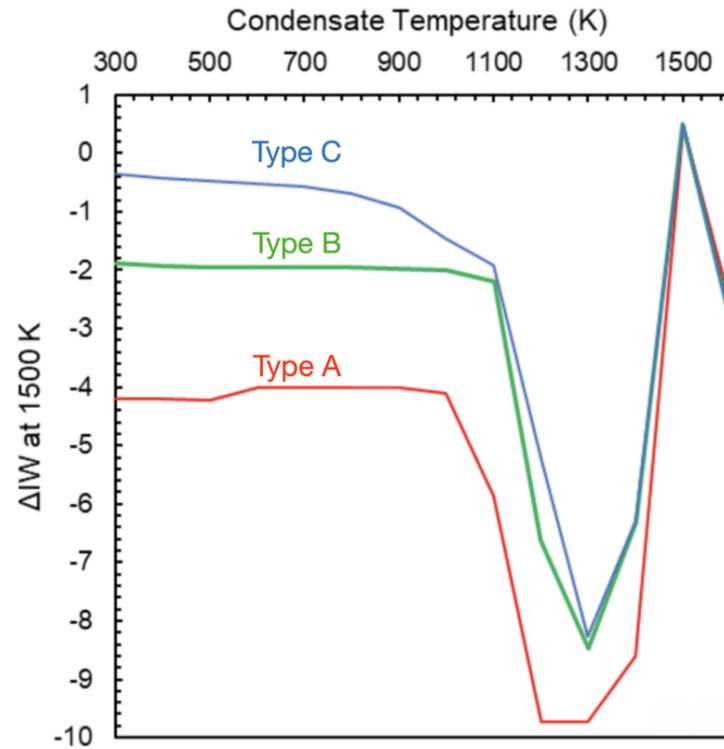
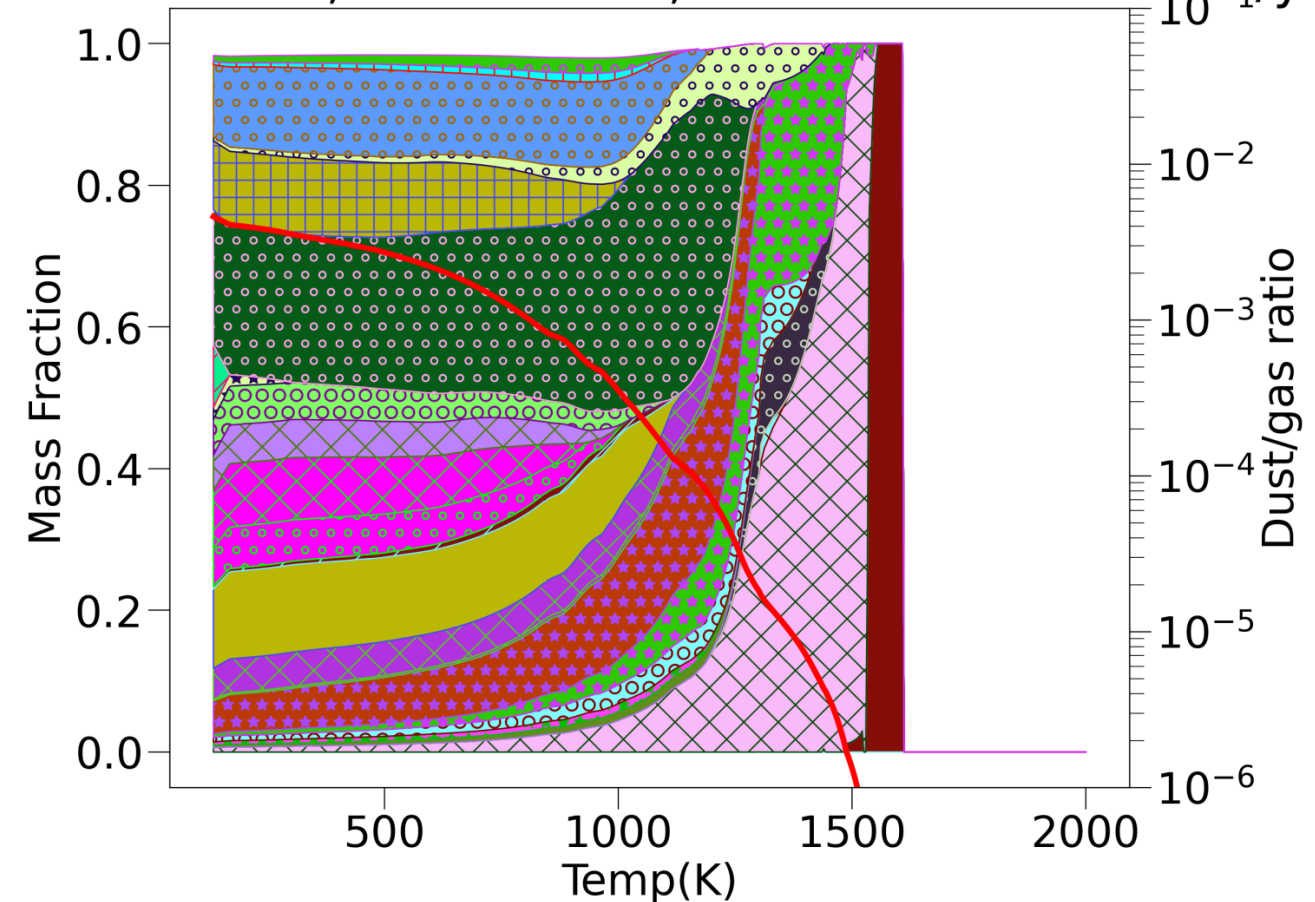


Fig. 14 Equivalent fo2 of re-equilibrated mineralogies for the three types A,B and C. The X axis stands for the temperature at which condensates are considered, while the Y axis gives the equivalent fo2 (with respect to the iron-wustite buffer). Here the types A,B,C are computed using the fast nebular reaction case.

Type C

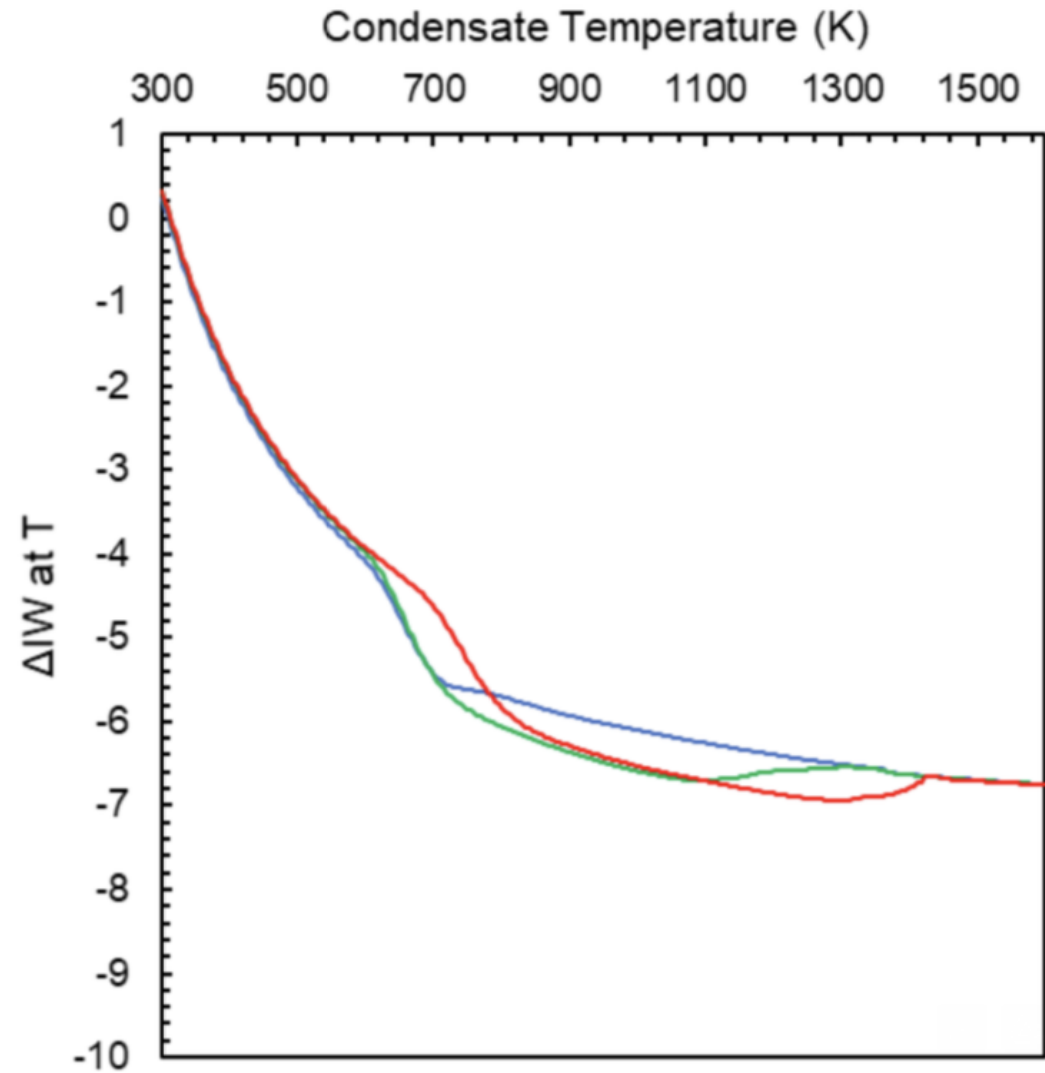
R=10.0 microns, P=1e-05bar, Cool Rate=19000 K/yr



Al2O3(cr),Corund

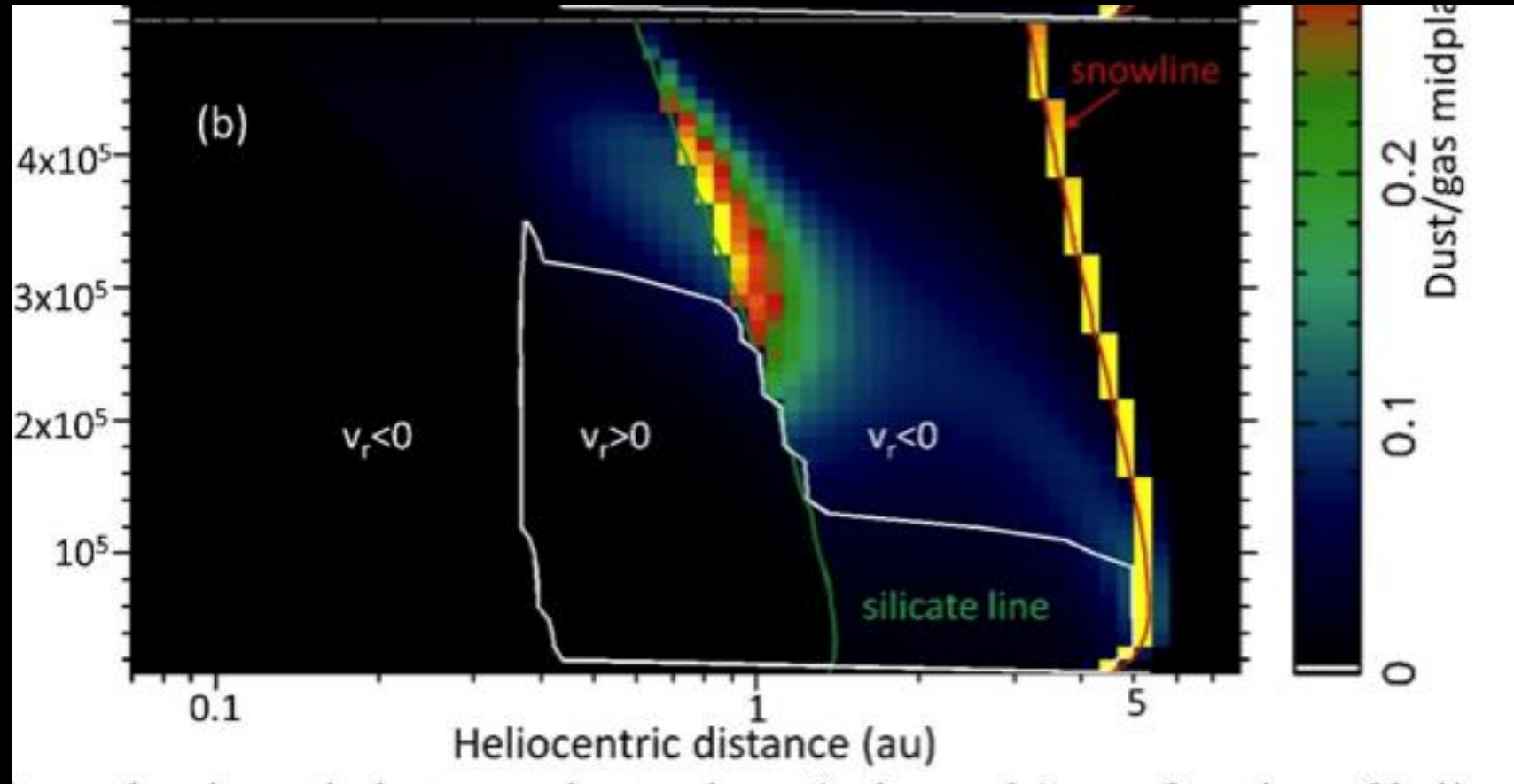
Fe3O4(cr),Magnet

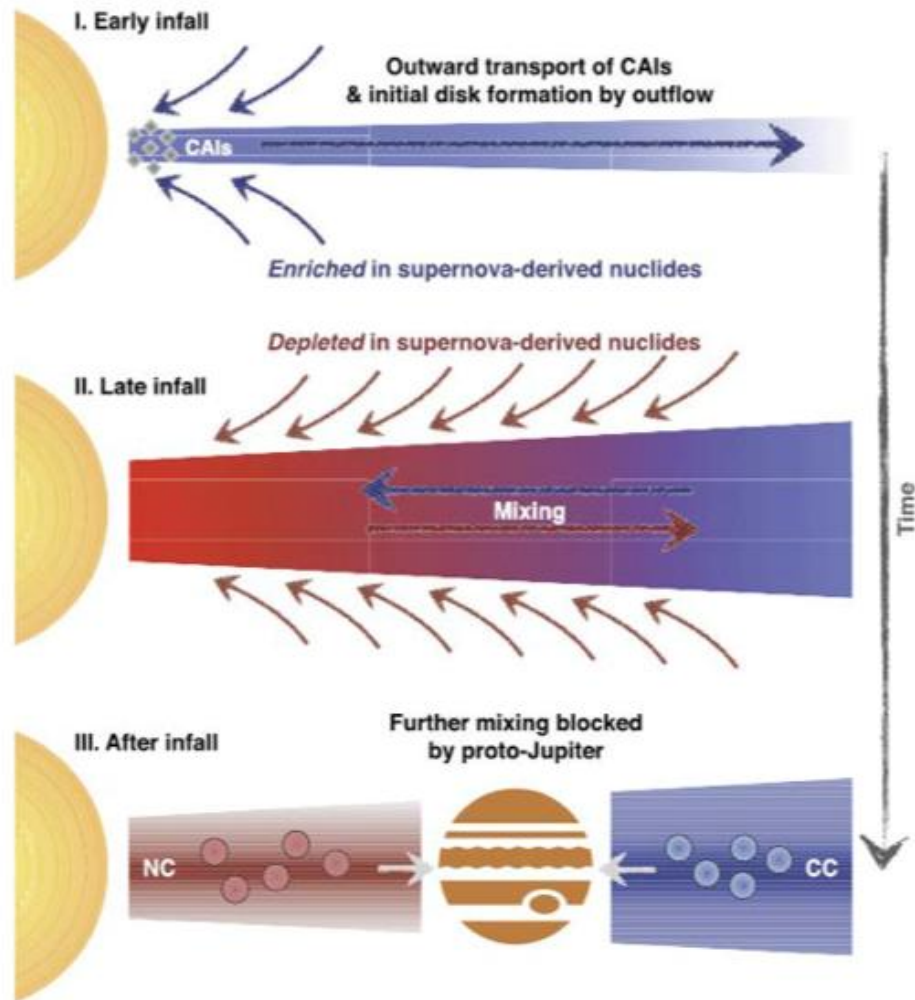
But the TRUE fO_2 is :



Very different
From mineral
Assemblages

The model of planetesimals formation in 2 sites (Morbidelli et al., 2022)





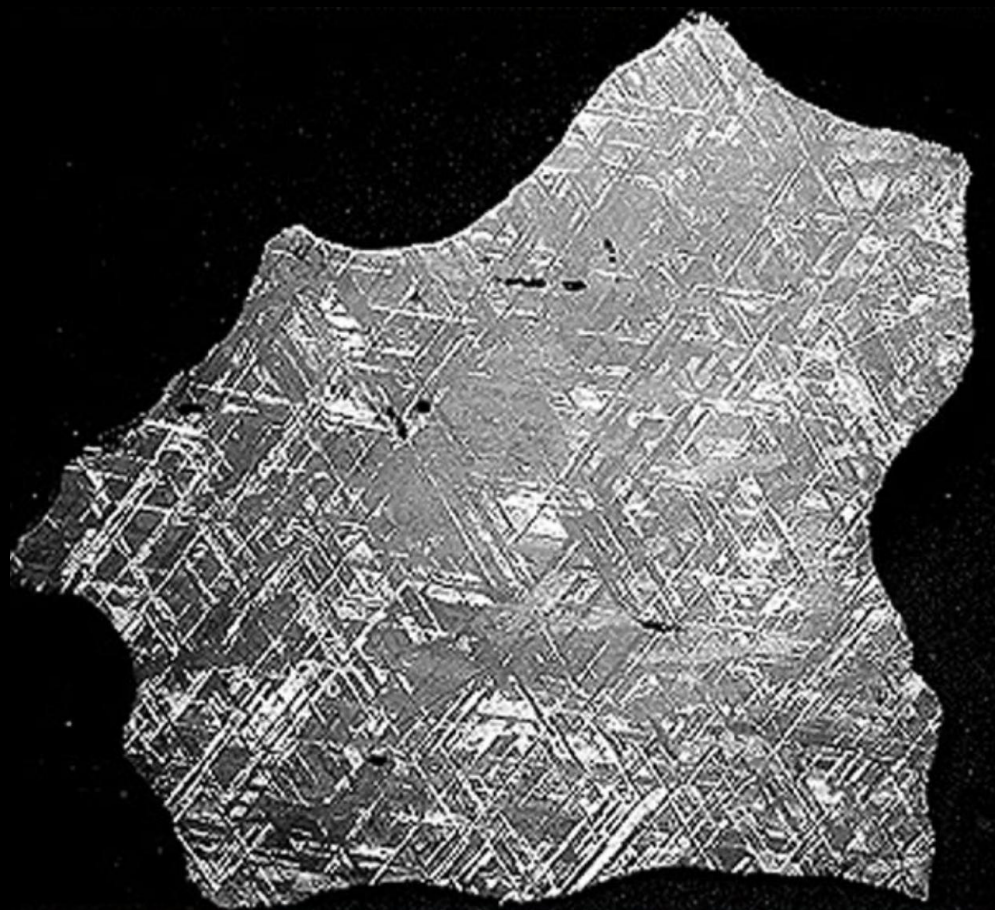
⇒ NC planetesimals should form
in a water free environment

⇒ NC population should be
« oxygen poor »
=>reduced

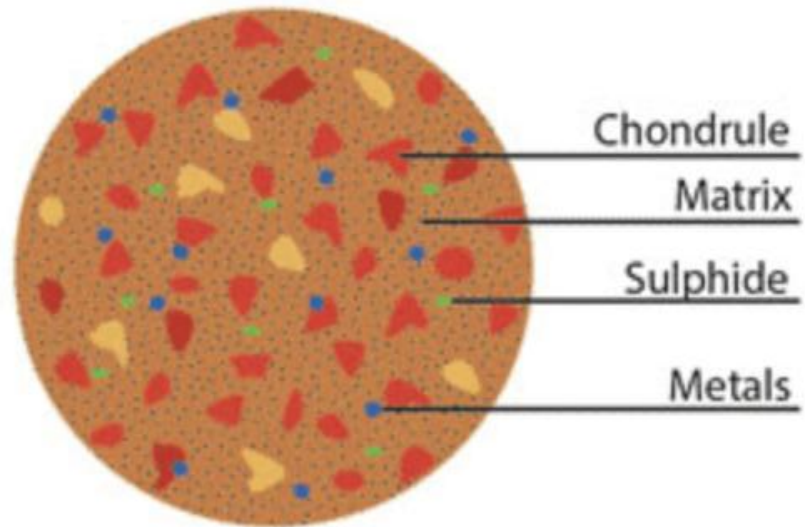
Fig. 10. Origin of the isotopic dichotomy. Left: Scheme of the accretion of material of changing isotopic composition in the inner part of the disk, as the disk is radially spreading, from [Nanne et al. \(2019\)](#). This established an isotopic gradient throughout the disk which is then turned into a dichotomy by the formation of early planetesimals at two distinct sites ([Morbidelli et al. 2022](#)) and the establishment of a barrier against radial drift of dust, here symbolized by Jupiter (see Sect. 4.2). Right: Isotopic composition in $\Delta^{95}\text{Mo}$ of CAIs ([Brennecka et al. 2020](#)), showing that the shift from the original isotopic composition toward the NC composition started to occur while condensation of calcium-aluminum inclusions was still ongoing.

A 'stone in the shoe' => Grewal 2024 paper

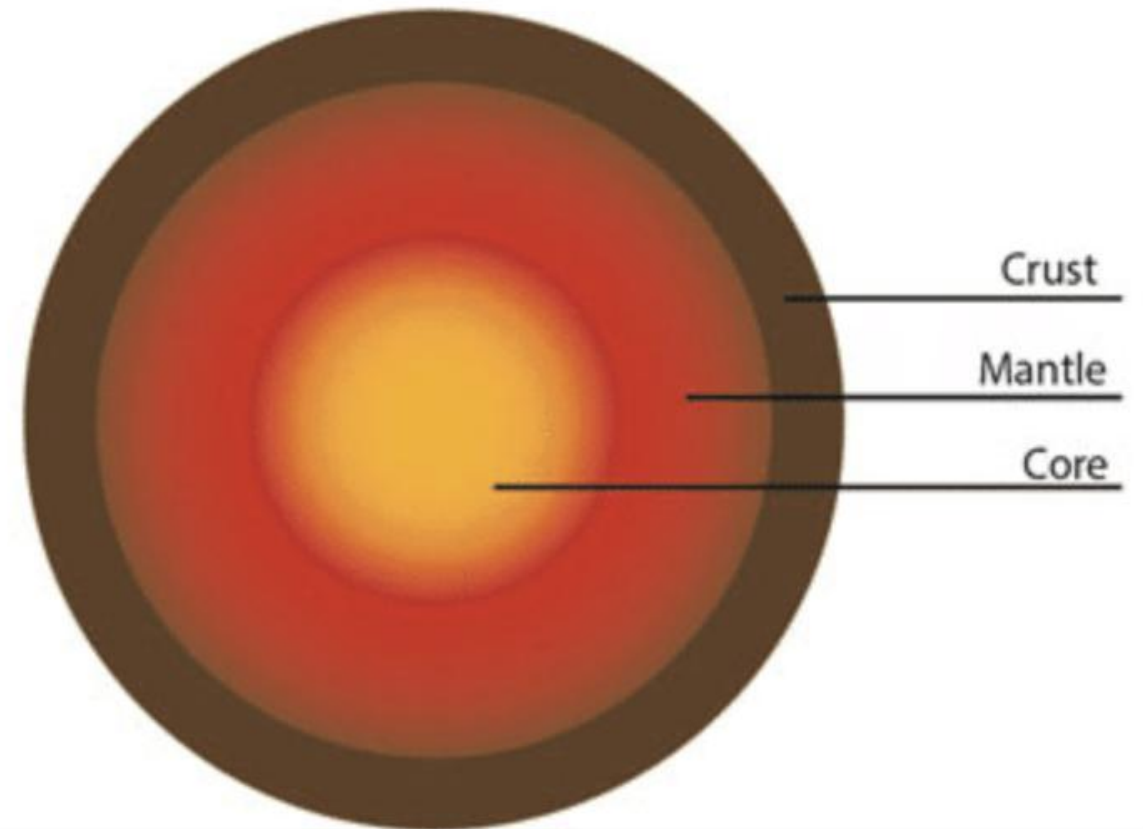
- ⇒ Interested in Iron meteorites
- ⇒ (cores of an old population of differentiated planetesimals)
- ⇒ Very old (comparable to CAIs age)

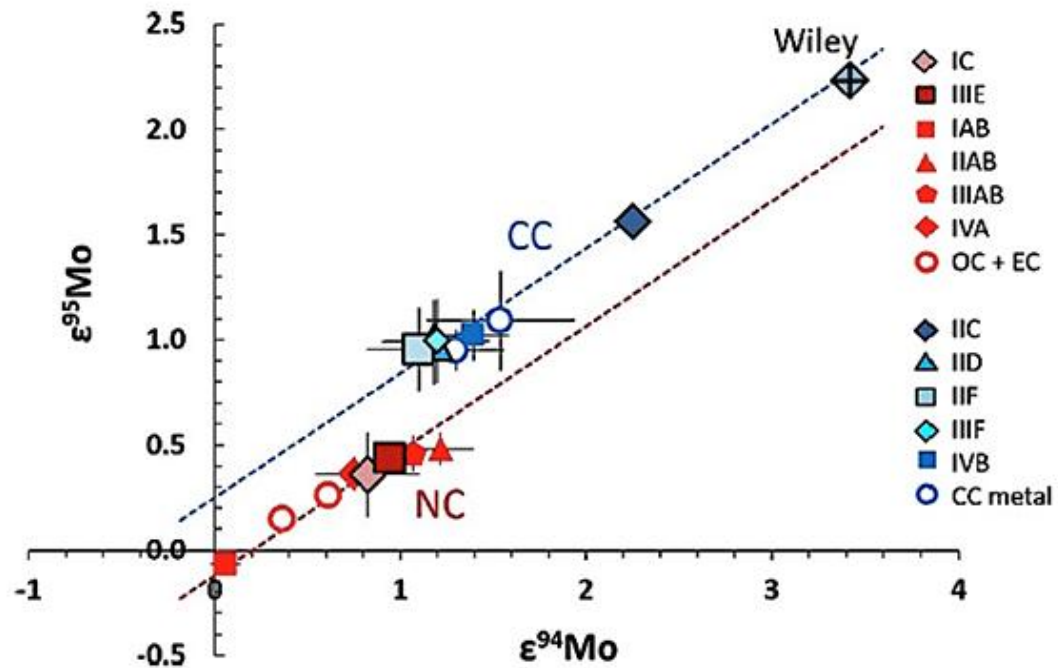


Undifferentiated asteroids

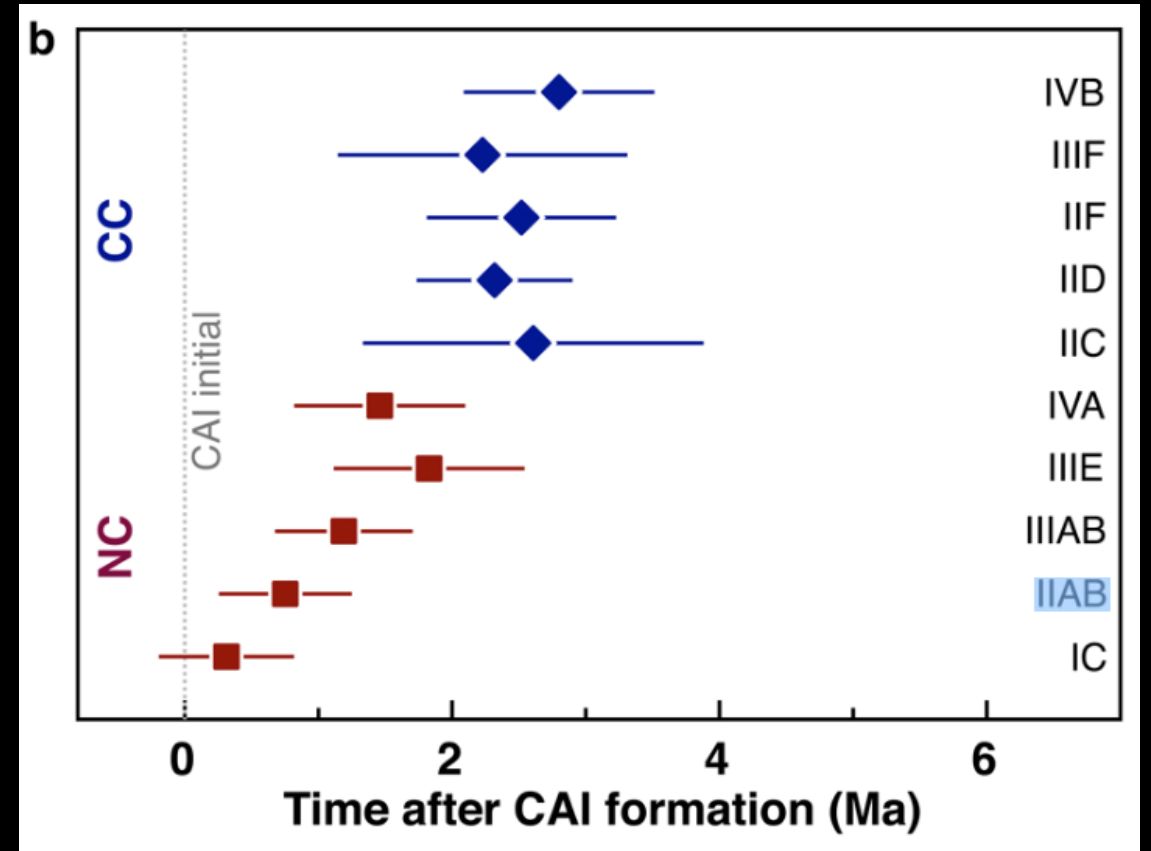


Differentiated asteroids and planets





Scott et al., 2022

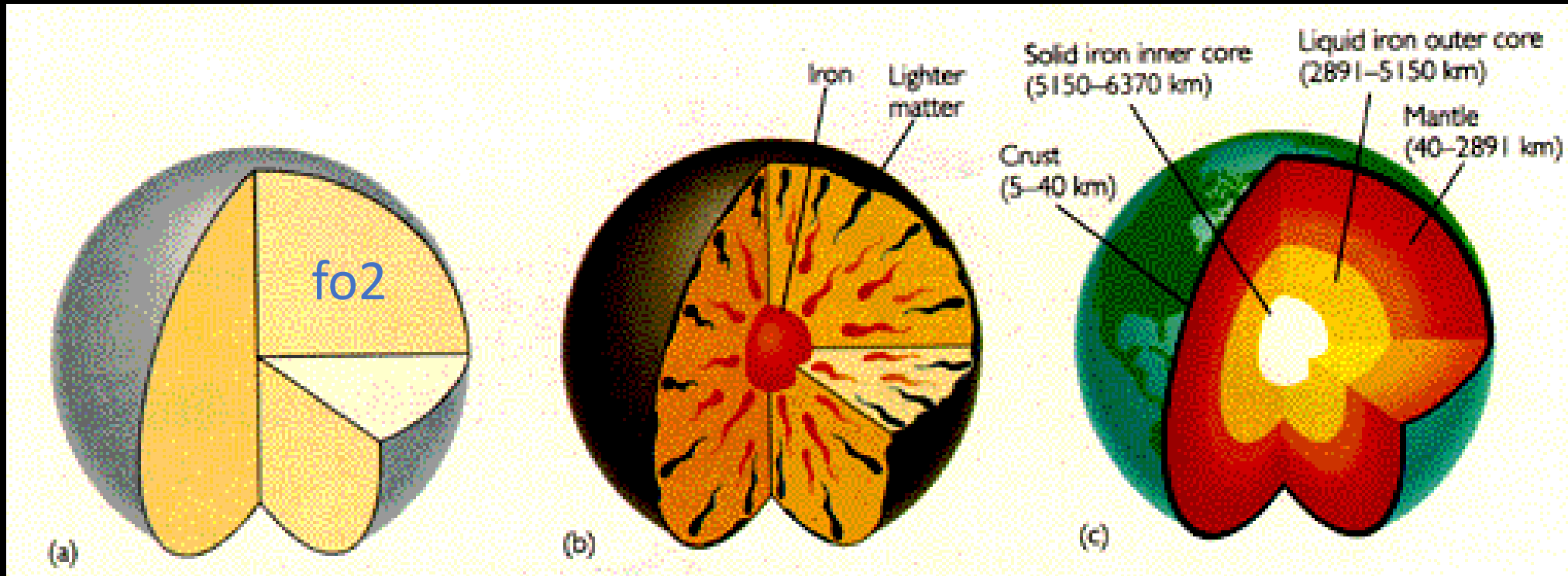


Kruijet 2024, age of differentiation
Of magmatic iron meteorites

The Oxidation state of Iron meteorite :

It is possible to determine the oxidation state of the PARENT BODY of iron meteorites by measure their Iron/Nickel and Cobalt/Nickel ratio

⇒ Their ratio depend on the amount of oxygen during differentiation..



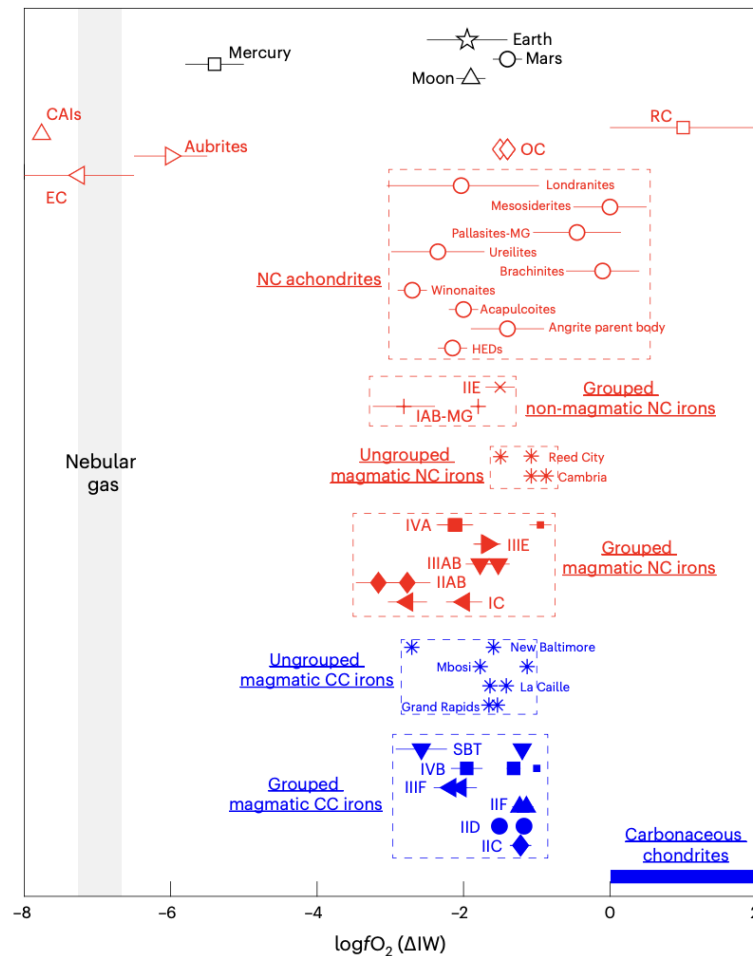


Fig. 3 | Variations in the oxidation states of various Solar System objects and reservoirs. The fO_2 of all rocky bodies in the NC (red) and CC (blue) reservoirs (except for the EC and aubrite parent bodies) are several orders of magnitude higher than the nebular gas and CAIs⁴⁷. Grouped NC IMPBs are not drastically more reduced than their CC counterparts. The fO_2 of grouped NC IMPBs are similar to those of ungrouped IMPBs, non-magmatic irons, OCs and several other groups of achondrites from the NC reservoir. The fO_2 prevailing during core–mantle differentiation of Earth (final event), Mars and the Moon also lie within the range of grouped NC IMPBs and other oxidized NC planetesimals. The two symbols for each grouped and ungrouped magmatic iron represent fO_2 calculated using their Fe/Ni and Fe/Co ratios. The smaller symbols for IVA and IVB groups represent fO_2 estimates from previous studies^{18,29}. Error bars for grouped and ungrouped magmatic irons represent 1σ deviation from the mean obtained by the propagation of uncertainty from individual terms in the fO_2 calculation of equation (2). The plotted data are reported in Extended Data Tables 2–4.

Oxidation state of Iron NC and CC Meteorites is similar !

⇒ NC Iron meteorites are not particularly « less oxidized » Than CC meteorites

⇒ Grewal concludes that NC formed At the snow line in the presence of Liquid/solid water

Kinetic condensation offers a possible way (?) to reconcile

⇒ Kinetic condensations shows that rapid condensation may lead to Oxidized state, if accretion occurs in an hydrogen rich environment

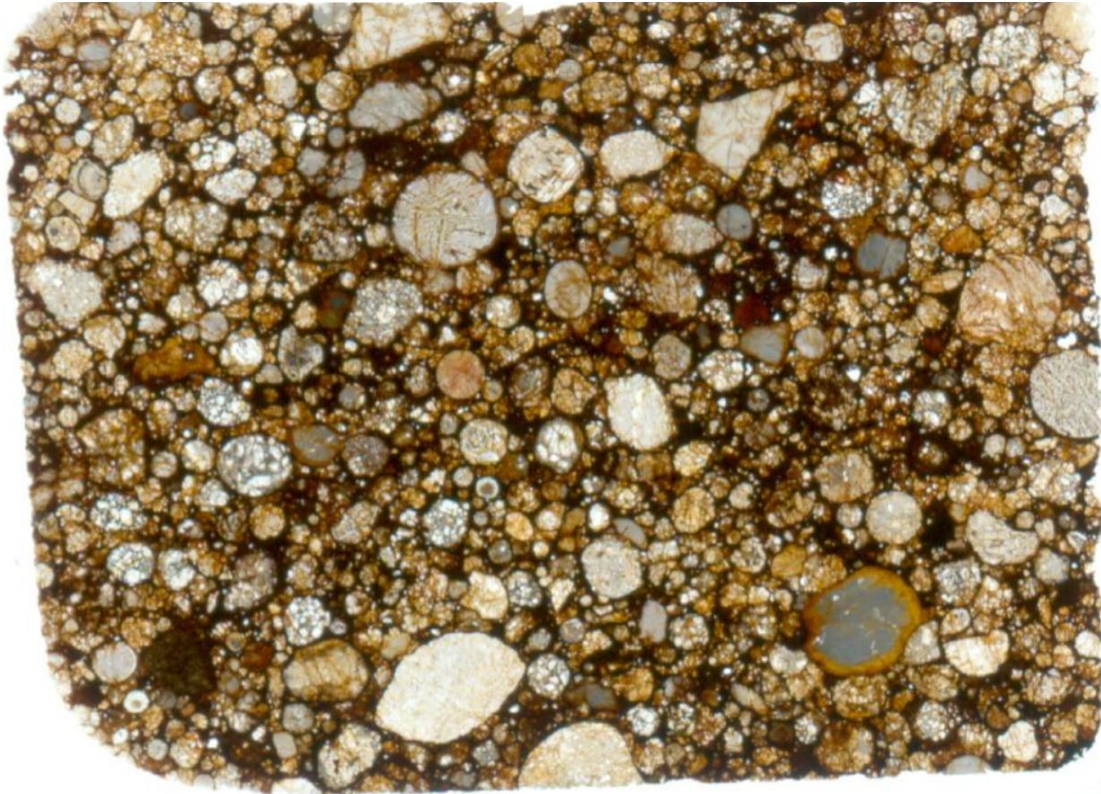
⇒ The Oxidation state is more a sign of the « out of equilibrium » nature Of the condensation process , rather than the Oxygen environnement

=> Heat and Cool my open a solution

We know there are heating and cooling processes in the early S.S.

=> Example : chondrules

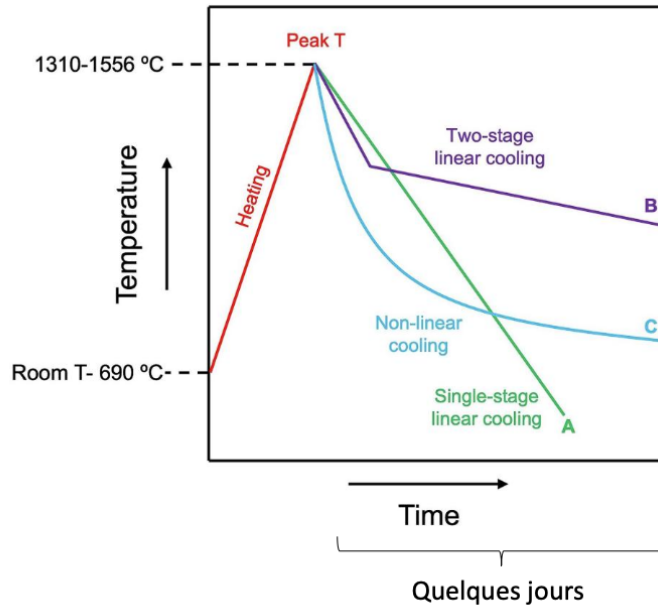
Les chondres



Molten silicate beads
heated > 1500 K

Histoire thermique des chondres

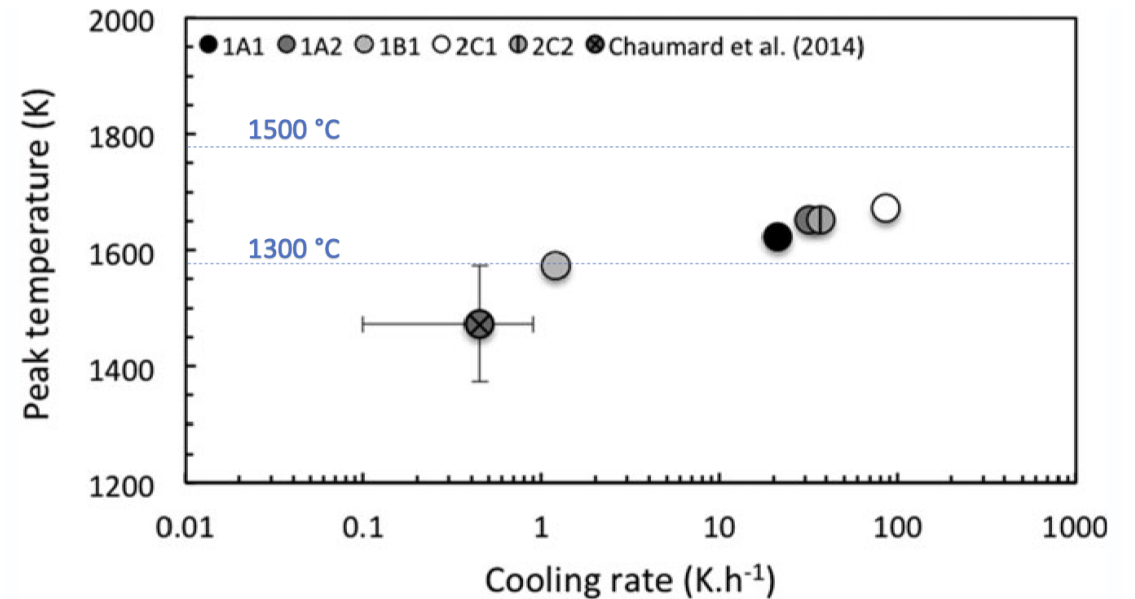
Smith and Jones, 2024



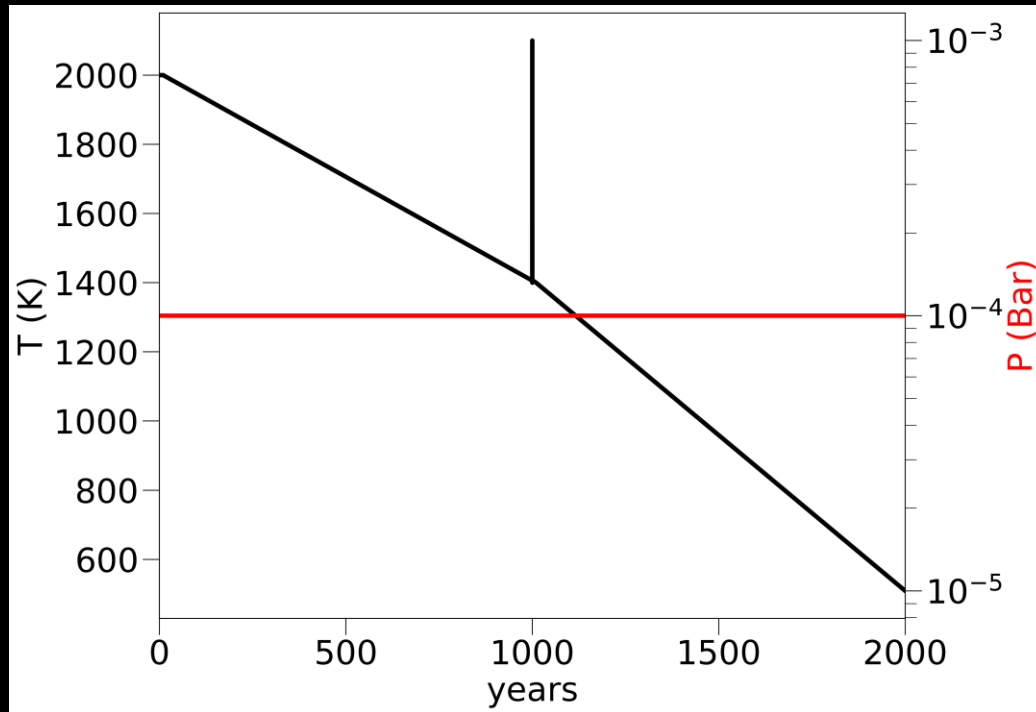
Expériences de laboratoire visant à reproduire la texture, la minéralogie et la chimie des chondres

Taux de refroidissement de 30 and 90 °C/h à 1310–1507 °C, 6 °C/hr à <1200 °C

Chaumard et al. (2018): analyse de grains de métal dans ou près des chondres

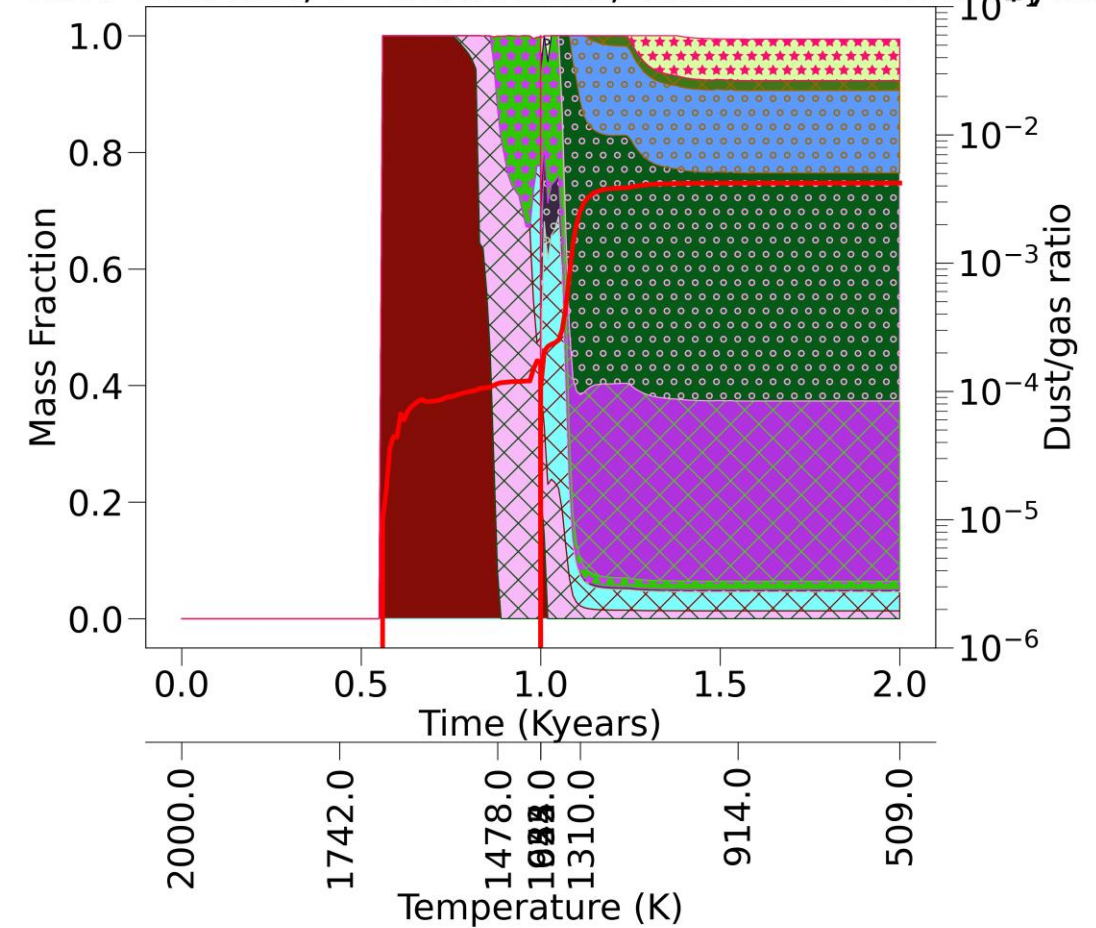


THERMAL PULSE 1: in a hot disk

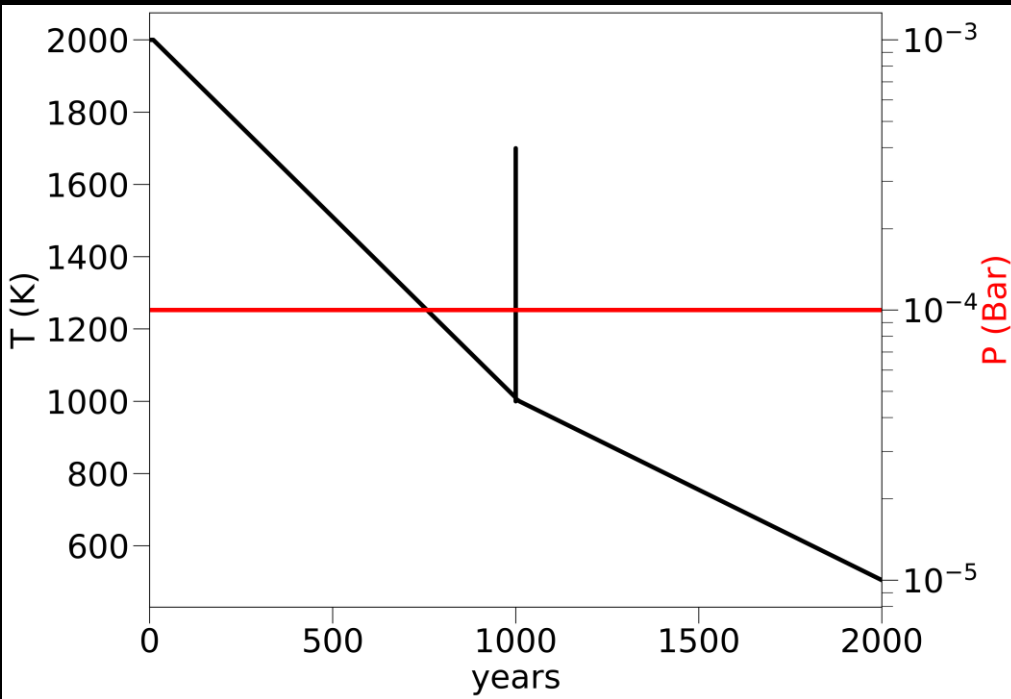


Reduced mineralogy form
 \Rightarrow Close to enstatite.

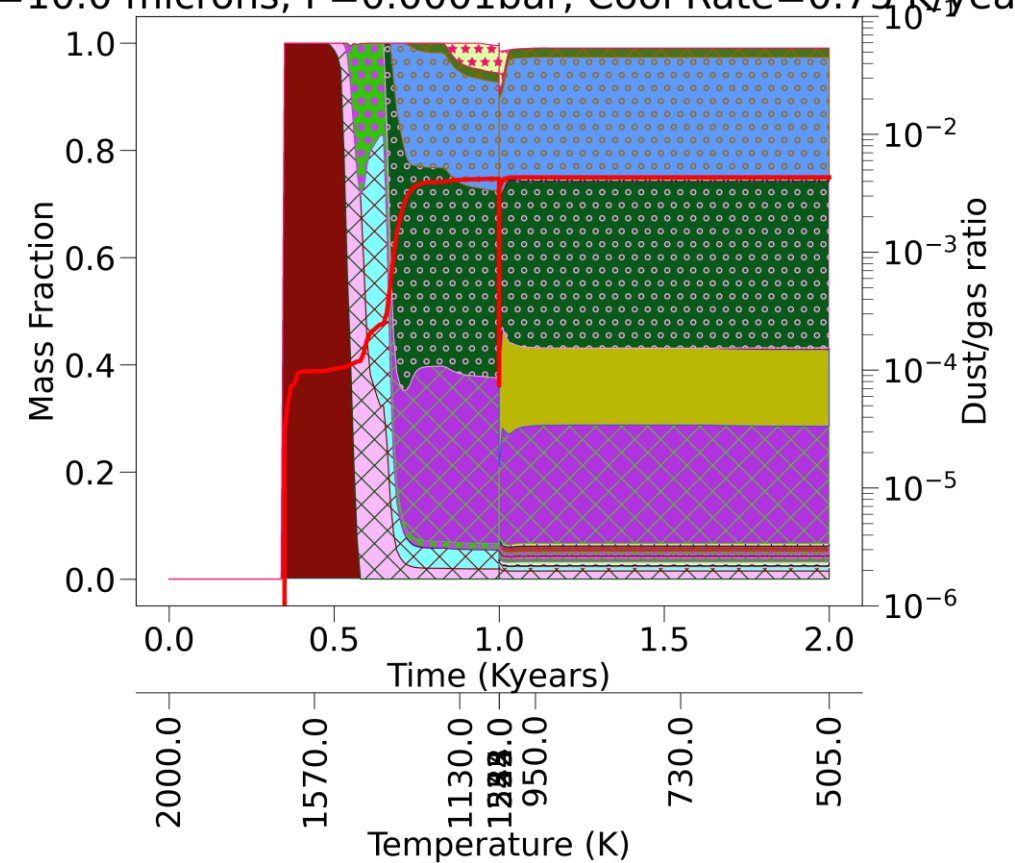
$R=10.0$ microns, $P=0.0001$ bar, Cool Rate= 0.75 K/year



THERMAL PULSE 2 : in a warm disk

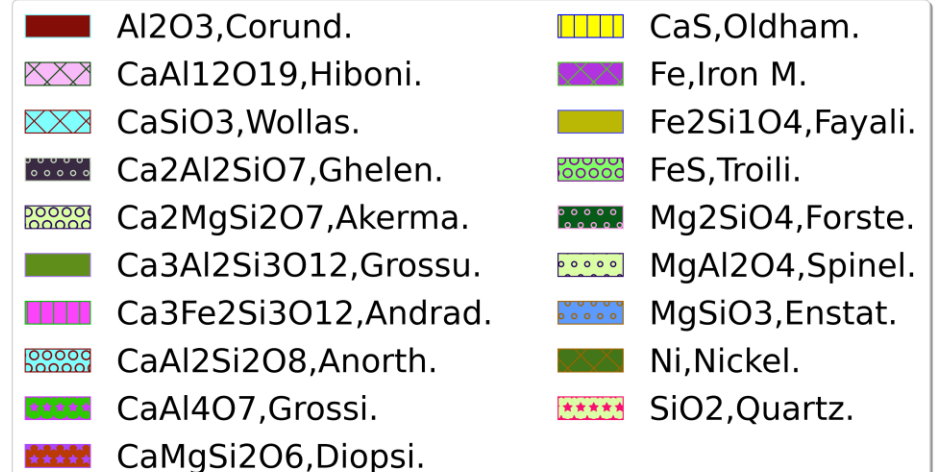


$R=10.0$ microns, $P=0.0001$ bar, Cool Rate= 0.75 K/year

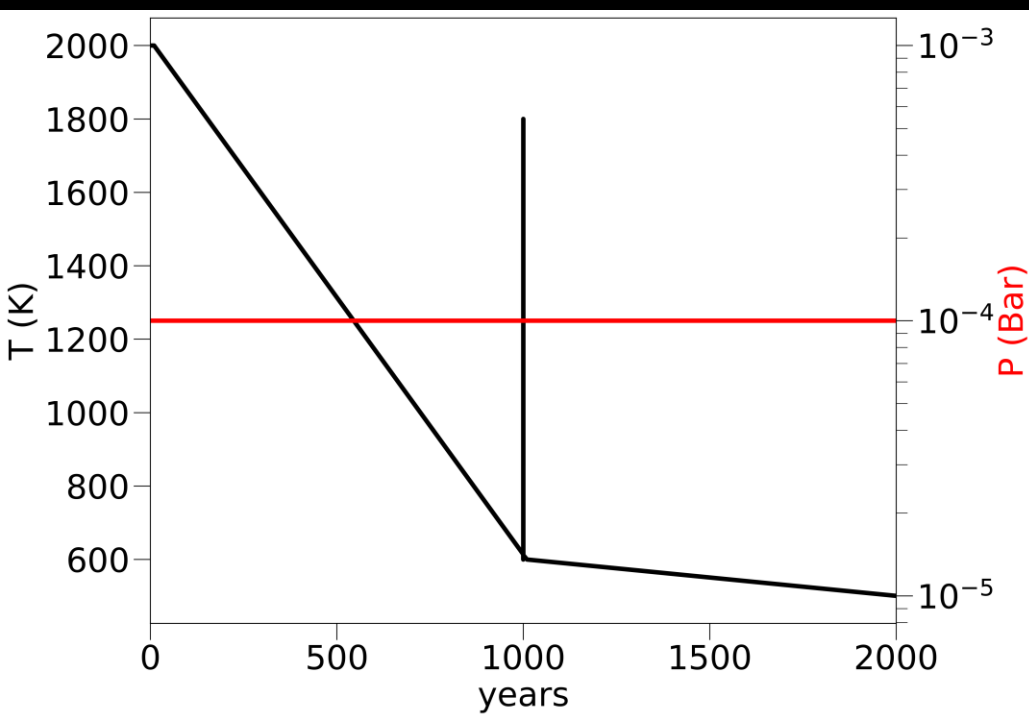


Produce a mineralogy close to ordinary chondrites :

Presence of Fayalite + interestingly we have a little bit of sulfure trapped



THERMAL PULSE 3: in a cold disk



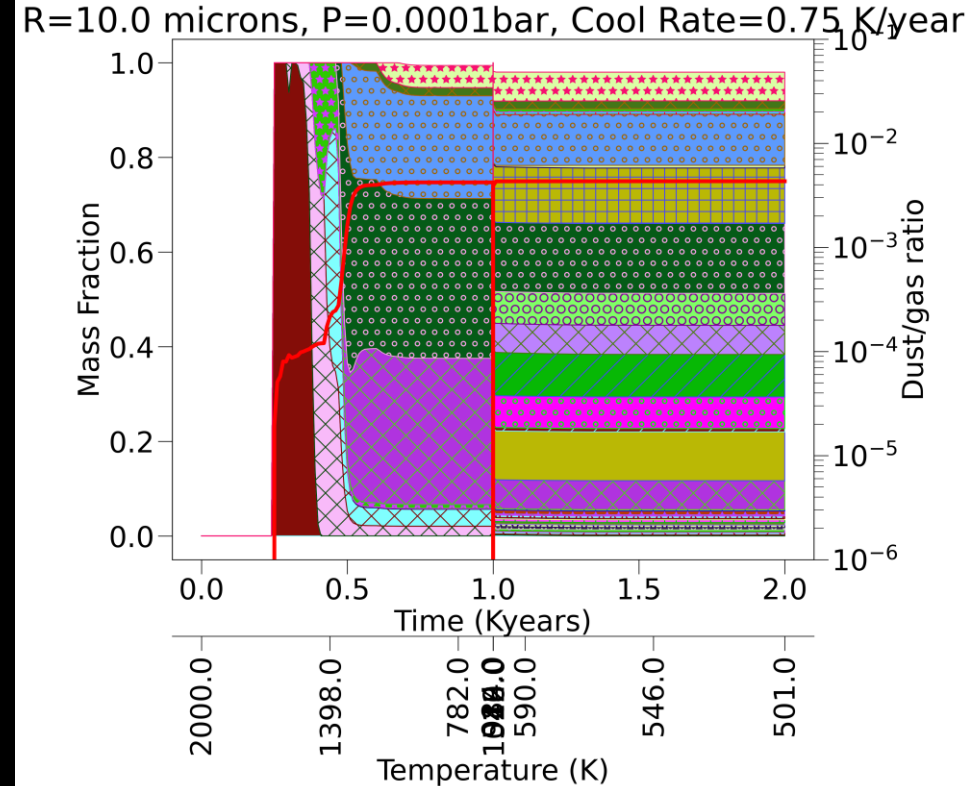
Produce a very rich and diverse mineralogy

And OXIDIZED mineralogy. :

Phyllosilicates :

Lizardite, greenalite, and a little bit of Talc

Very oxidized : Magnetite also



what would be the cause of these thermal pulses ?

How to change the oxidation state of the precursors ?

⇒ Problem somewhat similar to chondrules formatio...
but different epoch..

Impacts/collisions ?

Shockwaves in the disk ?

Electric discharge ?

Other ?

=> A problem of timescale and volume of material to processs

Early planetesimals shocks

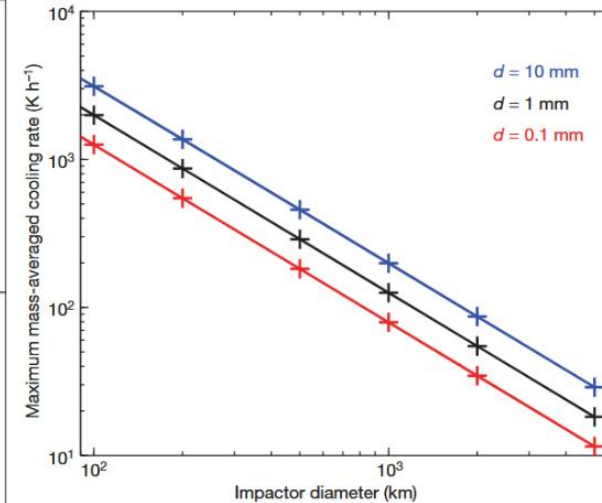
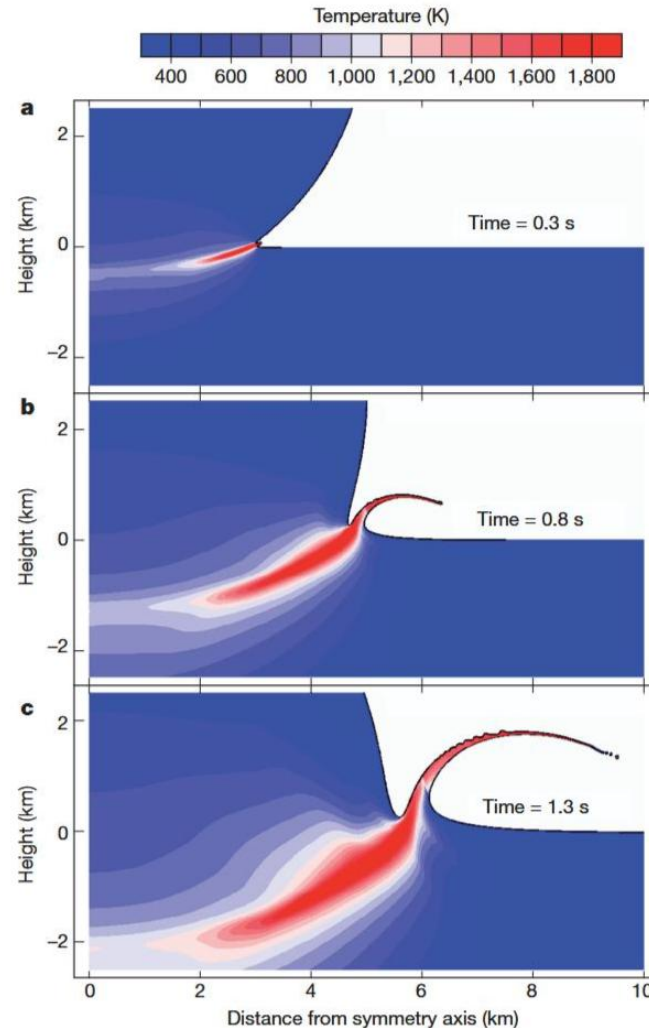
Impacts à haute vitesse entre corps plus ou moins grands peuvent fondre et éjecter dans l'espace une partie de la matière qui ensuite refroidit et cristallise rapidement.

Peut expliquer:

- Début retardé de formation des chondres
- Haute densité de matière pour limiter la dévolatilisation

Mais:

- Les premiers corps auraient dû être différenciés (voir cours #5), mais les chondres n'ont pas un grand déficit en Fe
- Grains précurseurs de chondres (voir séminaire)



Impact d'un objet de 10km à 3km/s sur objet de taille Lunaire
Johnson et al., 2015

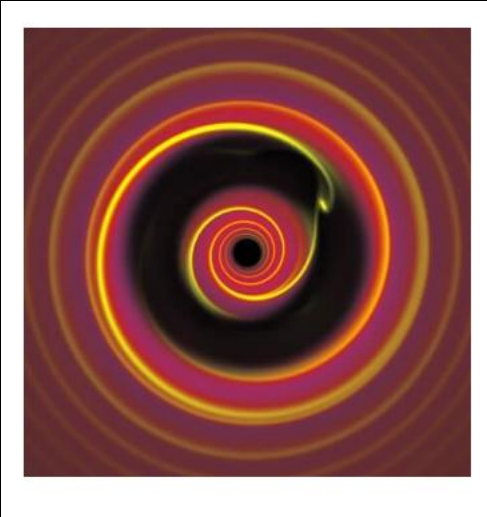
Voir aussi:

Asphaug et al., 2011

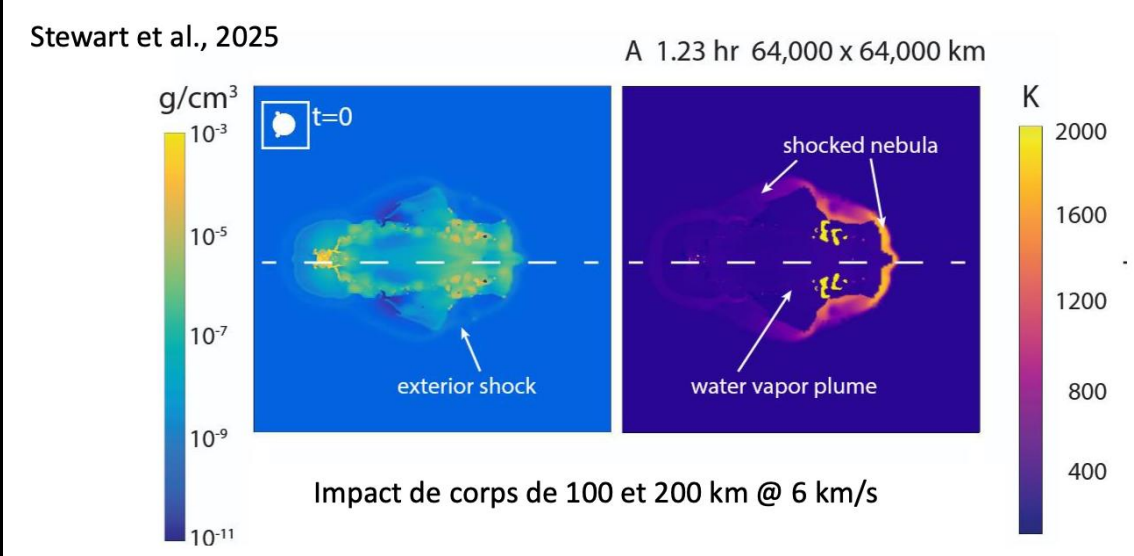
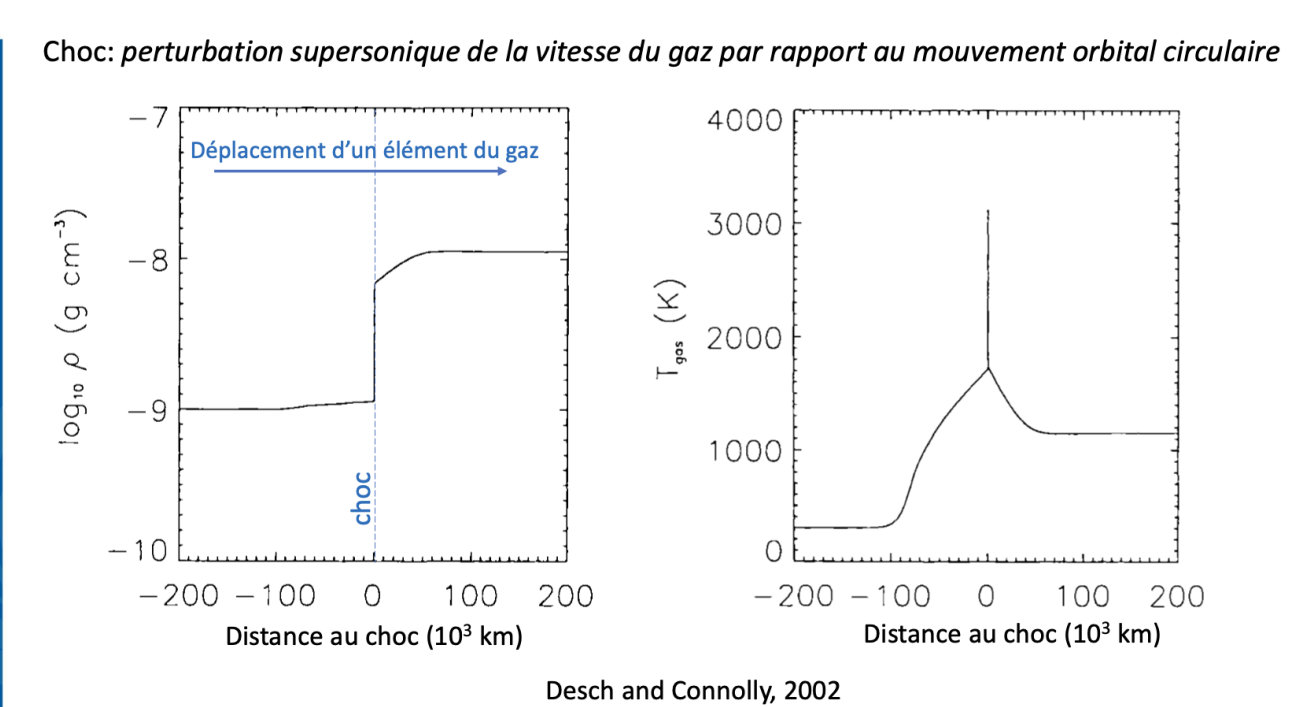
Dullemond et al., 2014, 2016

Need early big bodies to collide ... and vaporise... then recondense..
=> high velocity ? Not easy

Shockwave in the wake of planetary bodies



Masset et al., 2000



Steam shock

Electric discharge

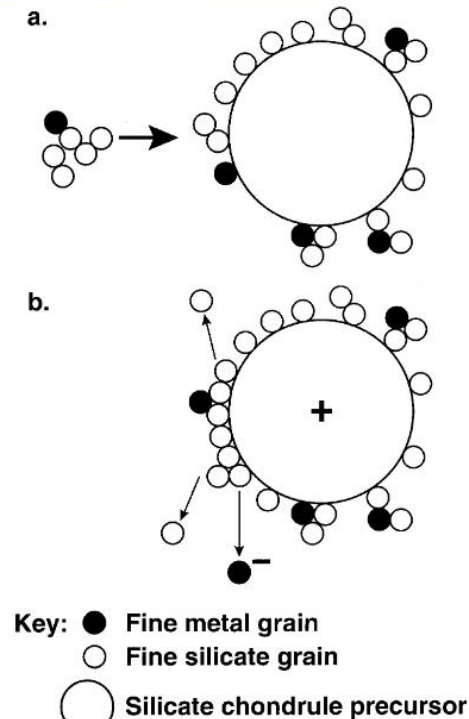
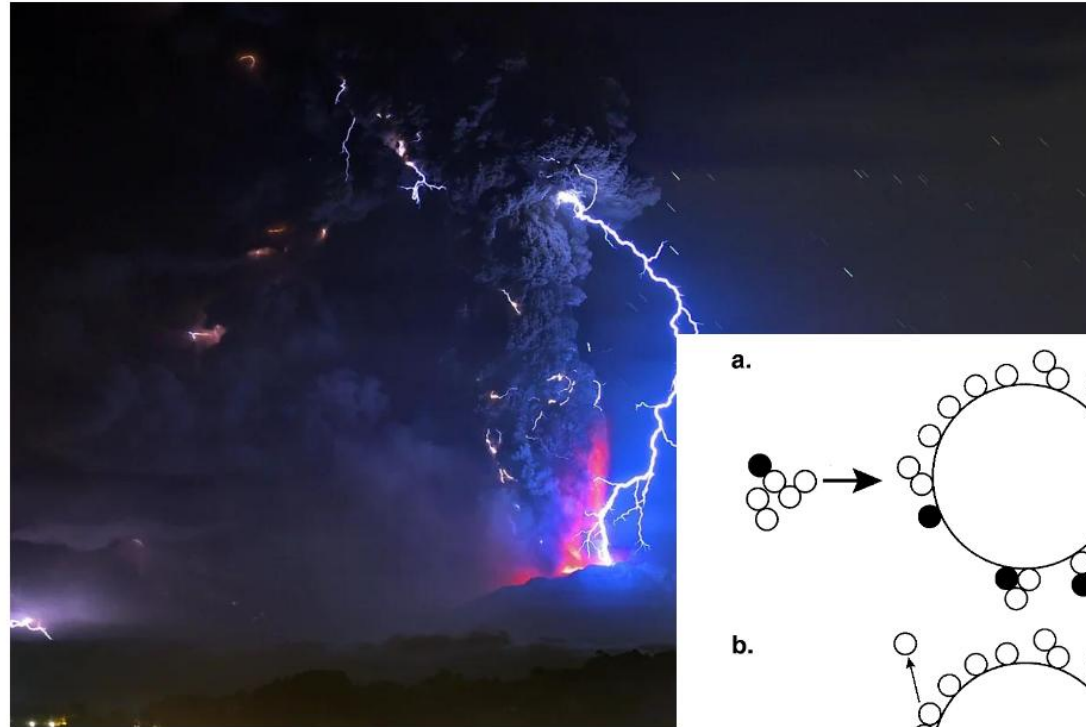
Desch et Cuzzi, 2000:

Analogie avec ce qu'il se passe lors des éruptions volcaniques: les collisions chargent électriquement les grains. S'il y a ségrégation des charges, la différence de potentiel peut devenir suffisamment grande pour déclencher une foudre

Compatible avec haute densité de poussières.

Mais processus inefficace car la section d'une foudre est très petite (~100 km)

Pourquoi un délai?



Pb : how to process big quantities of material...

How to heat and cool material rapidly AND early

An unclear situation

Most of heating cooling processes invoke a shock with a fully grown Planetary body...

⇒ Only the surface is affected and melted

⇒ Big planetary bodies appear late

➤ Difficult to process vast quantities of material early in the disk

➤ electric discharge is appealing : may happen any time .. BUT

➤ problem to process big quantities of material..

..=> This is still an open question

Condensation above the midplane in outflow..??? New speculative idea..
Needs exploration..

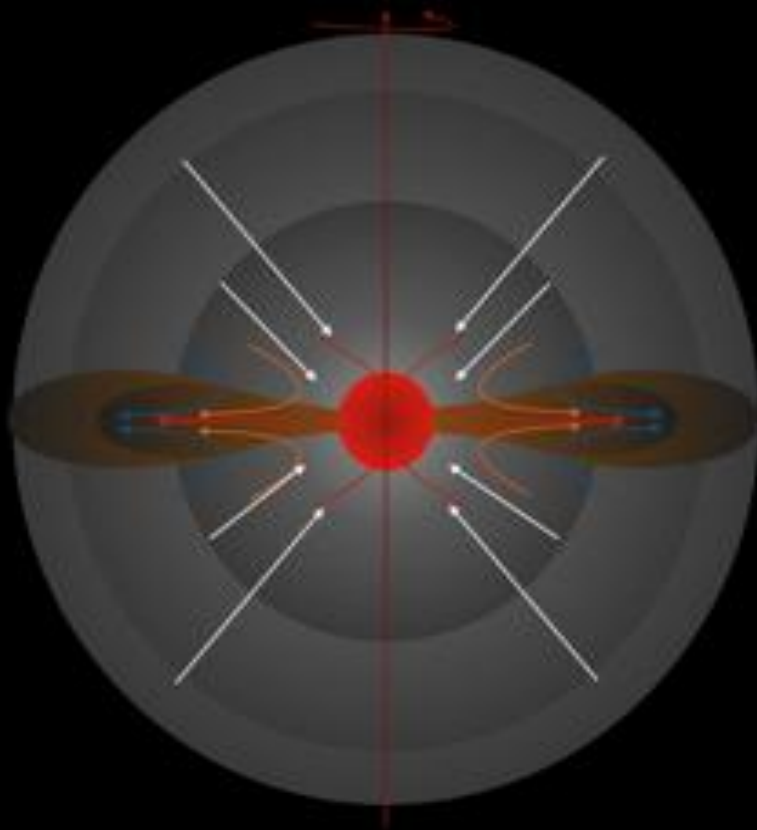
CONCLUSIONS

IMPORTANCE OF NON EQUILIBRIUM CONDENSATION

LOW PRESSURE / FAST COOLING

⇒ Equilibrium condensation give a very incomplete view

⇒ Origin of the 3 chondrites families



Oxidation state may reflect

out of equilibrium condensation processes rather than presence of water... a new idea that must be explored

⇒

Potential implication for the oxidation state of NC chondrites

And accretion of CC chondrites

⇒

Open questions